CRREL REPORT 95-22

Sensible Heat Flux Measurements Near a Cold Surface

Yin-Chao Yen

October 1995

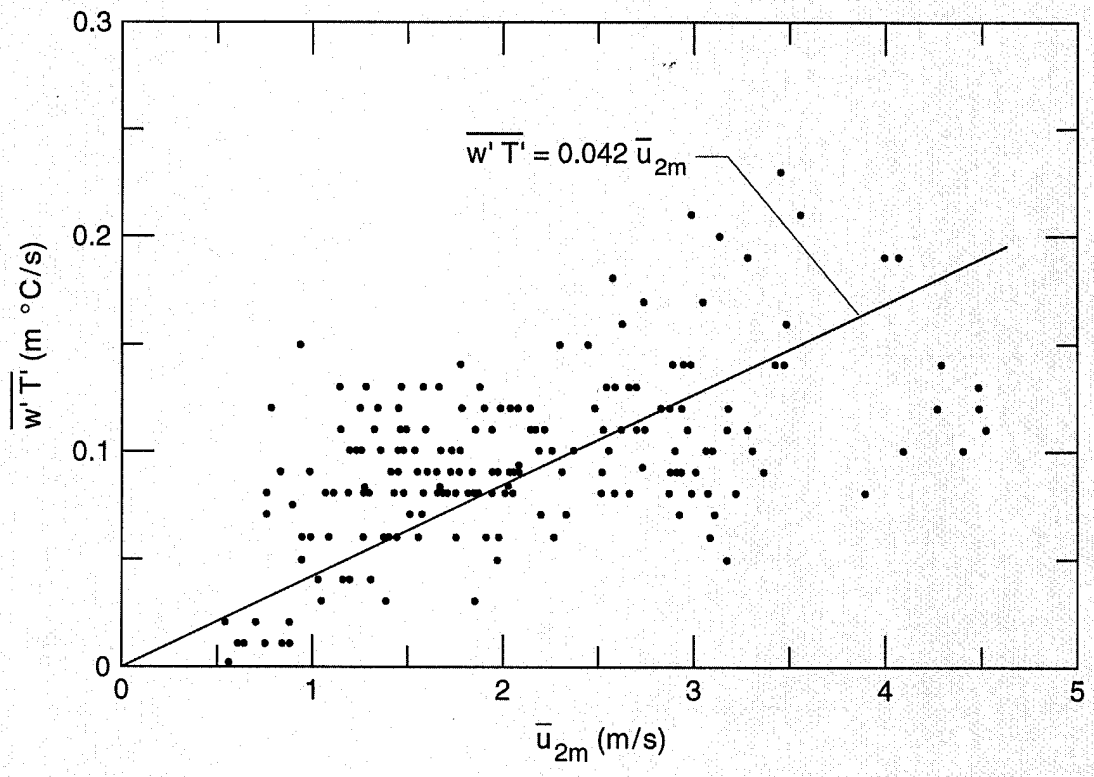

DISCLAIMER NOTICE

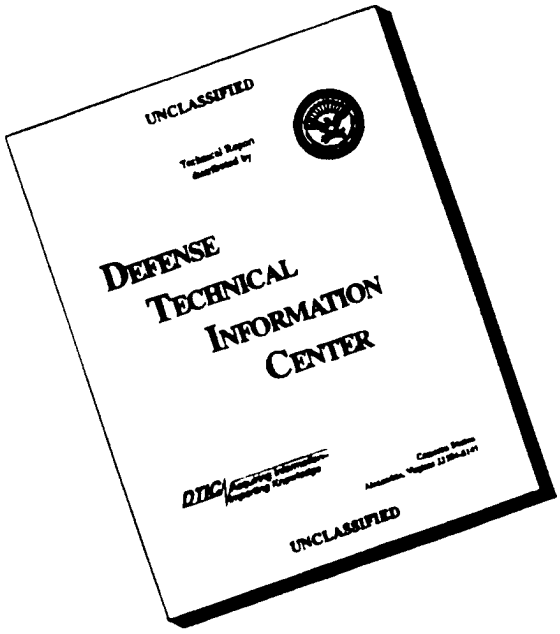

THIS DOCUMENT IS BEST QUALITY AVAILABLE. THE COPY FURNISHED TO DTIC CONTAINED A SIGNIFICANT NUMBER OF PAGES WHICH DO NOT REPRODUCE LEGIBLY.

Abstract

A unidirectional sonic anemometer with a fine-wire thermocouple in conjunction with a hot film anemometer were employed to measure the turbulent fluctuating velocities of w', u', and the fluctuating temperature T'. Covariances were evaluated to compute the turbulent heat flux and the friction velocity. Based on preliminary data, it can be noted that the values of fluctuating vertical velocity and temperature, the friction velocity, and the standard deviations of vertical and horizontal turbulent fluctuating velocities can all be correlated rather well with a single variable, i.e., the mean wind speed measured at a height of 2 m. In all the plots of friction velocity, vertical and horizontal turbulent fluctuating velocities, and the fluctuating vertical velocity and temperature vs. the mean wind speed at 2 m, the slopes are slightly lowered as the test season progressed from early summer to the winter. The most striking reduction can be observed in the case of the fluctuating vertical velocity and temperature vs. mean wind speed at 2 m. During the winter period, the slope is only about one third of that during the spring–summer period. In other words, under unstable conditions, for the same mean wind speed, the heat flux during the winter is only about one third of the flux that would have occurred during the spring–summer. Under stable conditions, the magnitude of the fluctuating vertical velocity and temperature is much smaller, and its value shows much greater dispersion. The values of fluctuating vertical velocity and temperature cannot be correlated in any meaningful manner, as is the case under unstable conditions, by the mean wind speed alone. Comparisons were made with the few existing measured data or with predictions from theoretical expressions, and they were found to be in fairly good agreement in some cases and to have large divergence in others.

Cover: Fluctuating vertical velocity and temperature ($\overline{w'T'}$) as a function of the mean wind speed ($\overline{u}_{2m}$).

For conversion of SI units to non-SI units of measurement consult ASTM Standard E380-93, *Standard Practice for Use of the International System of Units,* published by the American Society for Testing and Materials, 1916 Race St., Philadelphia, Pa. 19103.

CRREL Report 95-22

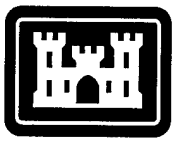

US Army Corps of Engineers
Cold Regions Research & Engineering Laboratory

Sensible Heat Flux Measurements Near a Cold Surface

Yin-Chao Yen

October 1995

Prepared for
OFFICE OF THE CHIEF OF ENGINEERS

PREFACE

This report was prepared by Dr. Yin-Chao Yen, Research Physical Scientist, Geophysical Sciences Division, Research and Engineering Directorate, U.S. Army Cold Regions Research and Engineering Laboratory, Hanover, New Hampshire.

Funding for this work was provided by the Office of the Chief of Engineers through DA Project 4A161102AT24, Task SS, Work Unit E09, *Surface Air Boundary Transfer Processes*, and DA Project 4A1623734DT08, *Combat Engineering Systems*.

This report was technically reviewed by Dr. Edgar L Andreas and Dr. Yoshisuke Nakano of CRREL. The author greatly appreciates Dr. Andreas's thorough and constructive review. He also wishes to thank David Fisk, John Fiori, Brian Harrington, and Frank Perron for their technical support, providing instrumentation, computer programming for data collection, and tower set-up for the sonic measurements. The author also thanks Dr. Harold S. Boyne, former chief of the Geophysical Sciences Branch, for his interest in and support of this new investigation.

CONTENTS

ILLUSTRATIONS

Figure Page

TABLES

Table

NOMENCLATURE

a	constant in eq 52
b	constant in eq 52
$CO_{w'T'}(f)$	cospectrum density of fluctuating vertical velocity and temperature
c_h, c_w, c_m	bulk transfer coefficient of heat, water vapor, and momentum
$c_{h,n}$, $c_{w,n}$, $c_{m,n}$	bulk transfer coefficient of heat, water vapor, and momentum under natural conditions
c_p	heat capacity
d	length of sonic path
E	water vapor flux
E', $E^{\sim}$	evaporation rate
e	vapor pressure
F_{ny}	Nyquist frequency
f	Coriolis parameter, turbulent frequency
g	gravitational acceleration
H	sensible heat flux
K_h, K_w, K_m	turbulent transfer coefficient of heat, water vapor, and momentum
k	Karman constant, thermal conductivity
L	Obukhov length, latent heat
L_s	latent heat of sublimation
M	molecular weight
M_{af}	snowmelt in forest canopy
n	dimensionless frequency
N	number of measurements
Nu	Nusselt number
Pr	Prandtl number
p	pressure, crown density of canopy
q	specific humidity
Q_h	sensible heat transfer
Q_e	latent heat transfer
Re	Reynolds number
Ri	Richardson number
Ri_f	Richardson flux number
Ri_c	critical Richardson number
Ri_b	bulk Richardson number
St	Stanton number
T, $\overline{T}$	air temperature, mean air temperature
T'	fluctuating temperature
t	time
u	horizontal wind speed
$\overline{u}$	mean horizontal wind speed
U	wind travel ($= u \cdot t$)
u_*	friction velocity
u,v,w	velocity components of the instantaneous wind vector ($u = \overline{u} + u'$, $v = \overline{v} + v'$, $w = \overline{w} + w'$)
$\overline{u},\overline{v},\overline{w}$	components of mean wind vector
$u',v';w'$	components of the fluctuating wind vector ($\overline{u'} = \overline{v'} = \overline{w'} = 0$)
x, y, z	Cartesian coordinate system

x, y	variable x and y
x', y'	fluctuating quantity in variable x and y
$\overline{x', y'}$	covariance in fluctuations of x' and y'
z	vertical distance from surface
z_o	roughness length or height
z/L	Monin-Obukhov stability parameter
—	overbar indicating time average
$\Delta\theta$	temperature difference
$\phi_{w'}(f)$	spectrum density of fluctuating vertical velocity
$\phi_{T'}(f)$	spectrum density of fluctuating temperature
ϕ_h, ϕ_w, ϕ_m	gradient functions for heat, water vapor, and momentum
ν	kinematic viscosity
ρ	density
$\sigma^2_{w'}, \overline{w'^2}$	variance of fluctuating vertical velocity
$\sigma^2_{T'}, \overline{T'^2}$	variance of fluctuating temperature
$\sigma_{w'}$	standard deviation of fluctuating vertical velocity
$\sigma_{u'}$	standard deviation of fluctuating horizontal velocity
$\sigma_{x'}$	standard deviation of x'
$\sigma_{x'_c}$	calculated standard deviation of x'
$\sigma_{x'_t}$	true value of standard deviation of x'
τ	Reynolds stress ($\tau = -\rho\overline{u'w'} = \rho u_*^2$)
∇^2	Laplacian operator

Subscripts

a	air
b	bulk
c	critical
f	flux
h	heat
m	momentum
n	neutral
o	at zero or at $z = z_o$
w	water vapor

Sensible Heat Flux Measurements Near A Cold Surface

YIN-CHAO YEN

I. GENERAL REVIEW OF PREVIOUS WORK

Eddy flux can be measured directly, but the method is expensive and complex and has generally been used only for short periods of time. For these reasons, estimates of these fluxes are generally obtained with the use of semi-empirical formulas involving simultaneous measurements of wind, temperature and humidity at several levels.

Field measurements have been conducted by numerous investigators, but the results usually differ from one another. In addition, most of the work was done over grass fields, crops, open water, ice, and glaciers. Swinbank (1951) reported the measurement of vertical transfer of heat and water vapor by eddies in the lower atmosphere. Thorpe et al. (1973) studied the eddy correlation measurements of evaporation and sensible heat flux over Arctic sea ice and reported bulk transfer coefficients of $c_n = 1.2 \times 10^{-3}$ and $c_w = 0.55 \times 10^{-3}$ with the Bowen ratio ranging from 1 to 15. Andreas et al. (1979) reported the measurement of turbulent heat flux from Arctic leads and suggested the sensible component of their turbulent heat flux can be predicted from bulk quantities. They suggested the results can be either expressed in an exponential relation, i.e., $Nu = 0.14\ Re_x^{0.72}$, or in a linear form as $Nu = 1.6 \times 10^{-3}\ Re_x + 1400$, where Nu is the Nusselt number and Re_x is the Reynolds number based on fetch across the leads. They stated, based on the similarity theory, that these expressions applied to the latent heat transfer as well. Over leads in winter, they found the sensible heat flux is two to four times greater than the latent heat flux. Wesley et al. (1970) employed a three-dimensional pressure-sphere anemometer and fast thermometer system to measure the vertical heat flux density in the atmosphere surface layer at 1–4 m above alta fescue and snap beans. They found the system is sufficiently small and has adequate high-frequency response and accuracy for eddy correlation measurements within 1 m of the surface.

Verma et al. (1978) reported measurements of turbulent exchange coefficient for sensible heat and water vapor over alfalfa and soybeans under conditions of advection. The exchange coefficient for sensible heat K_h is found to be generally greater than the exchange coefficient for water vapor K_w, which is in contradiction to the usual assumption of equality of K_h and K_w under nonadvective (lapse or unstable) conditions (i.e., the net transfer of both sensible heat and water vapor are directed away from the surface). On the other hand, under advective conditions heat and water vapor can be transferred in opposite directions. These results were confirmed by conclusions derived from a theoretical analysis by Warhaft (1976), who stated that the greatest departure of K_h/K_w from unity will occur where temperature and humidity gradients are of opposite signs.

Miyake et al. (1970) reported the comparison of turbulent fluxes over water determined by profile and eddy correlation techniques. The measurements were made with limited fetch and were under near-neutral conditions. However, the agreements were found to be well within the experimental error.

Hicks (1970) developed a general approach for the measurement of atmospheric fluxes near the surface; a covariance computer capable of accepting analog signals representing any two atmo-

spheric variables was described. It could compute the covariance in a frequency band governed at high frequencies by the sensor response times and at low frequencies by capacitive filters. This instrument, using vertical wind velocity as one input, has been successfully used for measurements of Reynolds stress and sensible and latent heat fluxes.

Though the necessity of measuring the vertical flux of heat and vapor, brought about by eddy measurement in the lower atmosphere, has long been recognized, Swinbank (1951) was the first to design an apparatus providing a continuous record (over a 5-minute interval) of the detailed structure of temperature, vapor pressure, and wind speed as well as its vertical component. He described the derivation of the vertical fluxes and presented an analysis of error estimation.

Dyer (1961) reported measurements of evaporation and heat transfer in the lower atmosphere by an automatic eddy-correlation technique that he proved to be practical and accurate for this type of measurement over a reasonably homogeneous surface. Under conditions of near-neutrality, the accuracy of the technique is not limited by response time over the range of wind speed normally encountered. With increasing atmospheric instability, the wind speed range can be further expanded and, unlike in the aerodynamic method, optimum performance is obtained at maximum instability. For measurements made at 4 m from the surface, Dyer indicated that minor surface irregularities of up to several tens of centimeters are clearly of no consequence, and if sufficient upwind fetch is available, even greater irregularities can be alleviated by increasing the height and period of observation.

Dyer (1967), in a study on the turbulent transport of heat and water vapor in an unstable atmosphere, indicated that the transfer mechanism for heat and water vapor are identical for a freely evaporating surface (i.e., $\phi_h = \phi_w$ where ϕ_h and ϕ_w are Monin–Obukhov universal functions for heat and water vapor gradients). Different expressions for ϕ_h and ϕ_w were presented dependent on the values of the stability parameter z/L (where z is the vertical distance from the surface at which the measurement is made, and L is the Obukhov length). He concluded that this finding is consistent with that from shape function analysis of the same data by Swinbank and Dyer (1967).

Hicks and Martin (1972) reported experimental results on atmospheric turbulent fluxes over snow. Their experiments were conducted under light wind along with a highly stable atmosphere near the snow surface. Fluxatrons developed by Hicks (1970) were used to determine these eddy fluxes. Hicks and Martin indicated that the use of eddy correlation technique to measure the fluxes of momentum, water vapor, and sensible heat over a snow or even an ice surface has been proved to be practical and to have a degree of accuracy satisfactory for many studies. They showed that snow surfaces are generally extremely smooth (not different from aerodynamic smoothness) with corresponding low friction velocities, so large deviations from atmospheric neutrality may be rather common. They claimed that direct measurement should be preferable to alternative techniques, based on assuming either the surface roughness or the similarity of transport mechanism. Low bulk transfer coefficients, based on data collected over Lake Mendota, Wisconsin, were expected after considering the influence of atmospheric stability on eddy diffusivity, and they reported fluxes of 9 W/m^2 for sensible heat and 22 W/m^2 for latent heat.

Swinbank (1968) derived a number of relationships based on dimensional analysis that connect the vertical fluxes of heat and horizontal momentum in the constant flux layer with other relevant variables. Experimental data taken under unstable conditions are used to test the correctness of the developed prediction relationship and its functional form. Swinbank found many dimensionless groups fit the data extremely well, with correlation coefficients in the range of 0.98–0.99. He reported that $\partial\overline{\theta}/\partial\overline{u}$ is height-dependent, indicating dissimilarity in respective transfer mechanisms, and concluded that any H, u_*, $\partial\overline{\theta}/\partial z$, and $\partial\overline{u}/\partial z$ at one level are sufficient to prescribe the heat transfer, the shearing stress, and the temperature and wind gradients throughout this constant flux layer over any uniform surface. Based on the predictive relationships and experimental data of half-hourly mean values, Swinbank concluded that up to a height of 16 m, the constant flux layer is

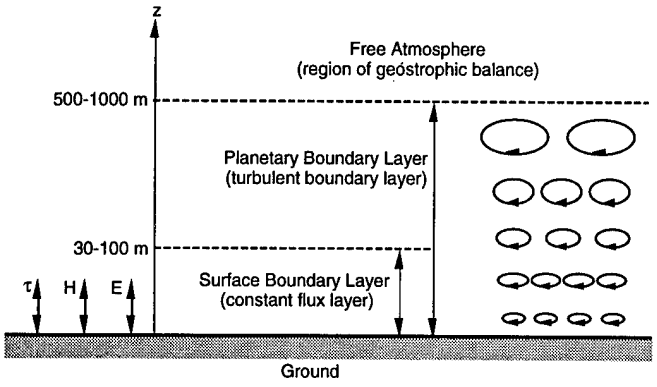

Figure 1. Vertical structure of the atmosphere (after Kai 1982).

homogeneous in behavior throughout its depth and provides no support to the suggestion that the layer may be divided into different regions according to stability.

Based on an exponential wind profile in a turbulent boundary layer with the air thermally stratified, Swinbank (1964) derived the vertical gradient as

$$\frac{\partial \bar{u}}{\partial z} = \frac{u_*}{kL}\left[1 - \exp\left(1 - \frac{z}{L}\right)\right]^{-1}$$

or in integrated form as

$$\bar{u}_2 - \bar{u}_1 = \frac{u_*}{k}\left\{-\frac{z_2 - z_1}{L} + \ln\left[\frac{\exp\left(-\frac{z_2}{L}\right) - 1}{\exp\left(-\frac{z_1}{L}\right) - 1}\right]\right\}$$

where k is the Karman constant. He claimed that this solution is expected to be applicable in all stabilities and to all heights below which the shearing stress and the vertical heat flux remain constant. Comparison with experimental data shows that buoyancy modifies the transfer of heat more strongly than does momentum, and the difference increases with height above the surface.

II. THEORETICAL RELATIONS AND METHOD OF ANALYSIS

The vertical structure of the atmosphere may be classified into three layers, as shown in Figure 1. The free atmosphere is free from the influences of surface friction, and its motion is treated as laminar flow. The planetary boundary layer, with considerable influence from surface friction, is analogous to the turbulent boundary layer found on a flat plate, and its motion is treated as turbulent flow. The surface boundary layer is the lowest 30 m or so of the planetary boundary layer, where the motion is controlled predominantly by the presence of surface friction. This layer is also referred to as the "constant flux layer," i.e., the vertical fluxes of physical properties by turbulence such as Reynolds stress and sensible heat flux are assumed to be constant to a good approximation.

A. General equation of motion

The structure of the surface boundary layer will first be explained with the aid of the fundamental principle governing the motion of the atmosphere near the surface of the ground. This principle is expressed by the Navier–Stokes equations for a viscous, incompressible, Newtonian medium in a uniform gravitational field and in a rotating system, which can be written in a rectangular coordinate system as

$$\frac{\partial u}{\partial t}+u\frac{\partial u}{\partial x}+v\frac{\partial u}{\partial y}+w\frac{\partial u}{\partial z}=-\frac{1}{\rho}\frac{\partial p}{\partial x}+\nu\nabla^2 u+fv$$

$$\frac{\partial v}{\partial t}+u\frac{\partial v}{\partial x}+v\frac{\partial v}{\partial y}+w\frac{\partial v}{\partial z}=-\frac{1}{\rho}\frac{\partial p}{\partial y}+\nu\nabla^2 v-fu \tag{1}$$

$$\frac{\partial w}{\partial t}+u\frac{\partial w}{\partial x}+v\frac{\partial w}{\partial y}+w\frac{\partial w}{\partial z}=-\frac{1}{\rho}\frac{\partial p}{\partial z}+\nu\nabla^2 w-g$$

where u, v, and w are the velocity components of the instantaneous wind vector, f is the Coriolis parameter, x, y, and z represent the Cartesian coordinate system, p is the pressure, ρ is the air density, g is the acceleration due to gravity, ν is the kinematic viscosity, and ∇^2 is the Laplacian operator.

Equation 1 describes the instantaneous motion of the atmosphere. However, in turbulent flow it is convenient to describe the mean rather than the instantaneous flow; this can be done by introducing components of the mean wind vector $(\overline{u},\overline{v},\overline{w})$ and the components of the turbulent wind vector, i.e.,

$$u=\overline{u}+u', \quad v=\overline{v}+v', \quad \text{and} \quad w=\overline{w}+w' \tag{2}$$

With the use of eq 2 and the application of the equation of continuity and averaging, eq 1 becomes

$$\frac{\partial \overline{u}}{\partial t}+\overline{u}\frac{\partial \overline{u}}{\partial x}+\overline{v}\frac{\partial \overline{u}}{\partial y}+\overline{w}\frac{\partial \overline{u}}{\partial z}+\frac{\partial}{\partial x}\overline{u'u'}+\frac{\partial}{\partial y}\overline{u'v'}+\frac{\partial}{\partial z}\overline{u'w'}=-\frac{1}{\rho}\frac{\partial \overline{p}}{\partial x}+\nu\nabla^2\overline{u}+f\overline{v}$$

$$\frac{\partial \overline{v}}{\partial t}+\overline{u}\frac{\partial \overline{v}}{\partial x}+\overline{v}\frac{\partial \overline{v}}{\partial y}+\overline{w}\frac{\partial \overline{v}}{\partial z}+\frac{\partial}{\partial x}\overline{v'u'}+\frac{\partial}{\partial y}\overline{v'v'}+\frac{\partial}{\partial z}\overline{v'w'}=-\frac{1}{\rho}\frac{\partial \overline{p}}{\partial y}+\nu\nabla^2\overline{v}-f\overline{u} \tag{3}$$

$$\frac{\partial \overline{w}}{\partial t}+\overline{u}\frac{\partial \overline{w}}{\partial x}+\overline{v}\frac{\partial \overline{w}}{\partial y}+\overline{w}\frac{\partial \overline{w}}{\partial z}+\frac{\partial}{\partial x}\overline{w'u'}+\frac{\partial}{\partial y}\overline{w'v'}+\frac{\partial}{\partial z}\overline{w'w'}=-\frac{1}{\rho}\frac{\partial \overline{p}}{\partial z}+\nu\nabla^2\overline{w}-g$$

Considering that the vertical variation within the planetary boundary layer is usually much greater than the horizontal variations and considering the case of steady state, eq 3 can be further simplified as

$$0=-\frac{1}{\rho}\frac{\partial \overline{p}}{\partial x}+\frac{1}{\rho}\frac{\partial}{\partial z}\left(-\rho\overline{u'w'}\right)+f\overline{v}$$

$$0=-\frac{1}{\rho}\frac{\partial \overline{p}}{\partial y}+\frac{1}{\rho}\frac{\partial}{\partial z}\left(-\rho\overline{v'w'}\right)-f\overline{u} \tag{4}$$

However, to a good approximation, near the surface the pressure gradient and the Coriolis force can be neglected and eq 4 can be written as

$$\frac{\partial}{\partial z}\left(-\rho\overline{u'w'}\right)=0 \tag{5}$$

or

$$\tau=-\rho\overline{u'w'}=\rho K_m\frac{\partial \overline{u}}{\partial z}=\text{Constant}, \tag{6}$$

in which K_m is the turbulent diffusivity of momentum. Equation 6 states simply that the Reynolds stress is a constant within the surface boundary layer and is independent of height. In a similar

manner, a sensible heat flux also independent of height can be derived as

$$H = \rho c_p \overline{w'T'} = \rho c_p K_h \frac{\partial \overline{T}}{\partial z} . \tag{7}$$

It states that the surface boundary layer is characterized essentially by the "constant flux layer."

B. Wind structure of the surface boundary layer

In the absence of buoyancy, the wind profile is given as

$$\frac{\partial \overline{u}}{\partial z} = \frac{u_*}{kz} , \tag{8}$$

where k is the Karman constant and u_* is the friction velocity defined by

$$u_* = \sqrt{\tau / \rho} = \sqrt{-\overline{u'w'}} . \tag{9}$$

Upon integrating, the mean wind speed is

$$\overline{u} = \frac{u_*}{k} \ln \frac{z}{z_o} . \tag{10}$$

u_* is employed as the reference velocity in the study of fluid flow over a rough surface. In general, it increases with both $\overline{u}$ and the roughness of the surface z_o, which is the height above the ground (or surface) where the wind speed vanishes (this is also known as the roughness length, a characteristic of the surface).

To take into account all stability conditions other than neutral, Monin and Obukhov (1954) modified eq 8 by introducing a universal function, $\phi_m(z/L)$, i.e.,

$$\frac{\partial \overline{u}}{\partial z} = \frac{u_*}{kz} \phi_m \left(\frac{z}{L} \right) \tag{11}$$

in which L is the Monin–Obukhov stability length defined as

$$L = -\frac{u_*^3 \rho c_p \overline{T}^3}{kgH} . \tag{12}$$

For the case of neutral stability or when $H = 0$, we have set $\phi_m(0) = 1$. If H is positive (the heat flux is directed from the ground upward), then z/L is negative, indicating an unstable condition. On the other hand, if H is negative, z/L is positive, indicating a stable condition.

The other two important stability parameters are the Richardson (Ri) and flux Richardson (Ri_f) numbers, which are respectively defined as

$$Ri = \frac{g}{\overline{T}} \left[\frac{\frac{\partial \overline{T}}{\partial z}}{\left(\frac{\partial \overline{u}}{\partial z} \right)^2} \right] \tag{13}$$

and

$$Ri_f = \frac{g}{\overline{T}} \frac{\overline{w'T'}}{\overline{u'w'} \frac{\partial \overline{u}}{\partial z}} = \frac{gH}{-\overline{T} c_p \tau \frac{\partial \overline{u}}{\partial z}} . \tag{14}$$

The sign of Ri is determined by the gradient of mean temperature, which is by convention negative in lapse and positive in inversion profiles. A value of Ri of zero, negative, or positive

indicates the conditions of neutral, unstable, or stable conditions, respectively. By a simple mathematical operation, the three parameters of Ri, Ri_f, and z/L are related to ϕ_m by

$$Ri_f = \frac{K_h}{K_m} Ri = \frac{1}{\phi_m}\left(\frac{z}{L}\right). \tag{15}$$

Similar expressions for mean temperature and humidity gradients can be written as

$$\frac{\partial \overline{T}}{\partial z} = -\frac{H}{\rho c_p k u_* z}\phi_h\left(\frac{z}{L}\right) \tag{16}$$

and

$$\frac{\partial \overline{q}}{\partial z} = -\frac{E}{\rho k u_* z}\phi_w\left(\frac{z}{L}\right), \tag{17}$$

where $\overline{q}$ is the mean specific humidity, E is the water vapor flux, and ϕ_h and ϕ_w are stability functions for heat and water vapor.

From the basic turbulent transfer equation, such as eq 8 for momentum and the following expressions of

$$\frac{\partial \overline{T}}{\partial z} = -\frac{H}{\rho c_p K_h} \tag{18}$$

for heat and

$$\frac{\partial \overline{q}}{\partial z} = -\frac{E}{\rho K_w} \tag{19}$$

for water vapor, we can relate the stability-related functions of ϕ_m, ϕ_h, and ϕ_w to the eddy turbulent transfer coefficients of K_h, K_m, and K_w by

$$\frac{K_w}{K_m} = \frac{\phi_m}{\phi_w} \quad \text{and} \quad \frac{K_h}{K_m} = \frac{\phi_m}{\phi_h}. \tag{20}$$

The final expression for H and E in terms of these stability-related functions and mean temperature, vapor pressure, and wind speed gradients can be written as

$$H = -\rho c_p k^2 z^2 \frac{\partial \overline{u}}{\partial z}\frac{\partial \overline{T}}{\partial z}\frac{1}{\phi_h \phi_m} \tag{21}$$

and

$$E = -\frac{0.622\rho}{p} k^2 z^2 \frac{\partial \overline{u}}{\partial z}\frac{\partial e}{\partial z}\frac{1}{\phi_w \phi_m}, \tag{22}$$

where e and p are vapor pressure in millibars. The value of 0.622 is the ratio of the molecular weight of water vapor to that of air. Therefore, by determining the gradients of mean wind speed, temperature, and specific humidity and the values of ϕ_h, ϕ_w, and ϕ_m, the sensible heat and water vapor flux can be evaluated.

C. Evaluation of ϕ_h, ϕ_w, and ϕ_m

A number of researchers have used the "similarity theory" developed by Monin–Obukhov (1954) as a framework to define the functions of ϕ_h, ϕ_w, and ϕ_m in terms of a dimensionless ratio of

z/L where L is invariant with height within the surface boundary layer. Experimental determinations of ϕ_h, ϕ_w, and ϕ_m are made by measuring the profiles of wind speed, temperature, humidity, and shear stress as well as the fluxes of heat and water vapor.

A great number of determinations of ϕ_h, ϕ_w, and ϕ_m have been reported in the literature (McVehil 1964, Dyer 1967, Dyer and Hicks 1970, Oke 1970, Webb 1970, Businger et al. 1971, Pruitt et al. 1971). However, due to logistical problems in choosing an ideal site to ensure the existence of the constant flux layer and other problems associated with the eddy correlation measurement technique, most of the results are not in agreement with each other. The following relationships have been adopted by Anderson (1976) to represent the majority of the determinations. For stable conditions, he suggested that

$$\phi_h = \phi_w = \phi_m = \left(1 + 5\frac{z}{L}\right), \tag{23}$$

which implies that $K_h = K_w = K_m$. For unstable conditions he recommended using

$$\phi_m = \left(1 - 16\frac{z}{L}\right)^{-1/4} \tag{24}$$

and

$$\phi_h = \phi_w = \left(1 - 16\frac{z}{L}\right)^{-1/2} \tag{25}$$

Equations 24 and 25 are commonly referred to as Businger–Dyer formulas. If the value of H and u_* are not available, the value of z/L can be related to a stability criterion that can be computed from commonly available data, i.e., $z/L = (K_h/K_m)\phi_m Ri$, then for stable conditions we have

$$\phi_h = \phi_w = \phi_m = 1 + 5\frac{z}{L} = (1 - 5Ri)^{-1} \tag{26}$$

and for unstable conditions

$$\phi_m = (1 - 16\,Ri)^{-1/4} \tag{27}$$

and

$$\phi_h = \phi_w = (1 - 16\,Ri)^{-1/2}. \tag{28}$$

At the geometric mean height of z_2 and z_1, the Richardson number can be evaluated from the expression

$$Ri = \frac{2g(z_2 - z_1)(\overline{T}_2 - \overline{T}_1)}{(\overline{T}_2 + \overline{T}_1)(\overline{u}_2 - \overline{u}_1)}. \tag{29}$$

With the values of ϕ_h, ϕ_w, and ϕ_m calculated from the determined value of Ri along with the values of wind speed, temperature, and specific humidity gradient, the sensible and water vapor flux can be determined from eq 21 and 22.

D. Critical Richardson number

Equation 26 can be written as

$$\phi_h = \phi_w = \phi_m = (1 - \alpha Ri)^{-1}. \tag{30}$$

As z/L (see eq 26) approaches infinity, the values of ϕ_h, ϕ_w, and ϕ_m also approach infinity. Therefore

αRi in eq 30 approaches unity or Ri approaches α^{-1}. A critical Ri is designated as $Ri_c = \alpha^{-1}$, beyond which no turbulent condition can exist.

In his original work, Richardson (1920) reported $Ri_c = 1.0$. However, most investigators (Businger 1973) indicate the value of Ri_c less than 1.0 and most likely in the range of 0.15 to 0.25. Brutsaert (1972) reported that the value of Ri_c increases for the case involving evaporation and radiation, but its increase will depend on atmospheric conditions. He stated that the value of Ri_c is not invariant but rather varies between 0.25, below which turbulence is very likely, and somewhat higher than 0.5, above which turbulence is not likely. In the case of a snow cover, the air temperature normally exceeds the snow surface temperature (during daylight hours) because of the surface's high albedo and high emissivity and its limiting temperature of 0°C, therefore stable conditions should predominate over the snow surface.

III. COMPUTATION OF TURBULENT FLUXES

A. Two-level measurement

Under conditions of neutral stability, and with the assumption of $K_h = K_m$, the sensible heat flux can be obtained from the expression

$$H = -\rho c_p k^2 \frac{(\bar{u}_2 - \bar{u}_1)(\bar{T}_2 - \bar{T}_1)}{\left(\ln \frac{z_2}{z_1}\right)^2}, \tag{31}$$

and similarly for $K_m = K_w$, we have

$$E = -\frac{\rho M_w}{p M_a} k^2 \frac{(\bar{u}_2 - \bar{u}_1)(e_2 - e_1)}{\left(\ln \frac{z_2}{z_1}\right)^2}, \tag{32}$$

where M_w and M_a are the molecular weight of water and air, respectively. Equations 21 and 22 can be used to determine H and E fluxes under all conditions in terms of stability-related functions of ϕ_h, ϕ_w and ϕ_m.

B. One-level measurement

In numerous cases, the measurements of wind, temperature, and humidity at two levels are not available. The basic equations for evaluating turbulent fluxes based on one-level measurement (essentially speaking, it is still a two-level measurement except one of the levels is located at the surface) are generally expressed in terms of bulk transfer coefficients of heat (c_h), water vapor (c_w), and momentum (c_m), defined as

$$H = -\rho c_p c_h \bar{u}(\bar{T} - \bar{T}_o), \tag{33}$$

$$E = -\frac{\rho}{p}\frac{M_w}{M_a} c_w \bar{u}(\bar{e} - \bar{e}_o), \tag{34}$$

and

$$\tau = u_*^2 \rho = \rho c_m \bar{u}^2, \tag{35}$$

where $\bar{e}$, $\bar{e}_o$ are the vapor pressure at z and the snow surface (or at $z = z_o$); and $\bar{T}$ and $\bar{T}_o$ are the mean air temperature at heights z and z_o.

To evaluate the bulk transfer coefficients, these coefficients under neutral conditions, i.e., $c_{h,n}$, $c_{w,n}$, and $c_{m,n}$, would have to be evaluated. If $K_h = K_w = K_m$ is assumed, then the following expression can be obtained:

$$c_{h,n} = c_{w,n} = c_{m,n} = \frac{k^2}{\left(\ln \frac{z}{z_o}\right)^2} \tag{36}$$

under unstable conditions. With the assumption of $c_h = c_w$, the expression of c_h and c_w in terms of c_m and $c_{m,n}$ can be written as

$$\frac{c_h}{c_{m,n}} = \frac{c_w}{c_{m,n}} = \left(\frac{c_m}{c_{m,n}}\right)^{1/2}\left[1 - \frac{2}{k} c_{m,n}^{1/2} \ln\left(\frac{1+x^2}{2}\right)\right]^{-1} \tag{37}$$

and

$$\frac{c_m}{c_{m,n}} = \left\{1 - \frac{c_{m,n}^{1/2}}{k}\left[\ln\left(\frac{1+x^2}{2}\right) + 2\ln\left(\frac{1+x}{2}\right) - 2\tan^{-1} x + \frac{\pi}{2}\right]\right\}^{-2}, \tag{38}$$

where x stands for $[1-\gamma(z/L)]^{1/4}$ and γ is a constant determined experimentally. To compute these ratios using observations at the surface and at height z, z/L can be related to a stability index such as bulk Richardson number, Ri_b, defined as

$$Ri_b = \frac{2gz\left(\overline{T} - \overline{T}_o\right)}{\left(\overline{T} + \overline{T}_o\right)\overline{u}^2}, \tag{39}$$

and the Obukhov length can be transformed as

$$L = \frac{c_m^{3/2}\,\overline{T}\,\overline{u}^2}{c_h k g\left(\overline{T} - \overline{T}_o\right)}. \tag{40}$$

The value of z/L can be related to Ri_b by

$$\frac{z}{L} = \frac{k\,c_h}{c_{m,n}^{3/2}\left(\frac{c_m}{c_{m,n}}\right)^{3/2}} Ri_b. \tag{41}$$

Lumley and Panofsky (1964) indicated that, for stable conditions, the log-linear profile is appropriate, and thus the dimensionless wind, temperature, and specific humidity gradients can be written respectively as

$$\frac{kz}{u_*}\frac{\partial \overline{u}}{\partial z} = 1 + \beta_m \frac{z}{L},$$

$$\frac{ku_*z}{-\frac{H}{\rho c_p}}\frac{\partial \overline{T}}{\partial z} = 1 + \beta_h \frac{z}{L}, \text{ and} \tag{42a,b,c}$$

$$\frac{ku_*z}{-\frac{E}{\rho}}\frac{\partial \overline{q}}{\partial z} = 1 + \beta_w \frac{z}{L},$$

where βs are treated as constant but not equal to each other even though Lumley and Panofsky have

set $\beta_m = \beta_h$. The bulk coefficient ratios corresponding to eq 42a,b,c can be derived and expressed as

$$\frac{c_m}{c_{m,n}} = \left[1 + \beta_m \frac{c_h}{c_{h,n}} \left(\frac{c_m}{c_{m,n}}\right)^{-3/2} Ri_b\right]^{-2},$$

$$\frac{c_h}{c_{h,n}} = \left(\frac{c_m}{c_{m,n}}\right)^{1/2} \left[1 + \beta_h \frac{c_h}{c_{h,n}} \left(\frac{c_m}{c_{m,n}}\right)^{-3/2} Ri_b\right]^{-1}, \text{ and} \qquad (43a,b,c)$$

$$\frac{c_h}{c_{h,n}} = \left(\frac{c_m}{c_{m,n}}\right)^{1/2} \left[1 + \beta_h \frac{c_h}{c_{h,n}} \left(\frac{c_m}{c_{m,n}}\right)^{-3/2} Ri_b\right]^{-1}.$$

Using eq 43a,b, a relation involving $c_m/c_{m,n}$ with β_m, β_h, and Ri_b can be derived as

$$\left(1 - \frac{\beta_m}{\beta_h}\right)\frac{c_m}{c_{m,n}} - 2\left(1 - \frac{\beta_m}{2\beta_h}\right)\left(\frac{c_m}{c_{m,n}}\right)^{1/2} + \left(1 - \frac{\beta_m^2}{\beta_h} Ri_b\right) = 0 . \qquad (44)$$

Figure 2 shows the ratio of the transfer coefficient to its neutral value over a wide range of Ri_b. It can be seen that, unlike the unstable case, the curves for the stable case calculated based on $\beta_m = 7$, $\beta_h = 11$, and $\beta_w = 20$ are independent of $c_{m,n}$. The sudden change of slope around $Ri_b = 0$ is due to the fact that the values of β_m and β_h are not equal to $\gamma/4$ and $\gamma/2$, respectively ($\gamma = 16$).

Deardorff (1968), for practical purposes, approximated the bulk transfer coefficient (over water) for the stable case by

$$\frac{c_m}{c_{m,n}} = \exp\left(-2\beta_m Ri_b\right),$$

$$\frac{c_h}{c_{h,n}} = \exp\left[-\left(\beta_m + \beta_h\right) Ri_b\right], \text{ and} \qquad (45a,b,c)$$

$$\frac{c_w}{c_{w,n}} = \exp\left[-\left(\beta_m + \beta_w\right) Ri_b\right],$$

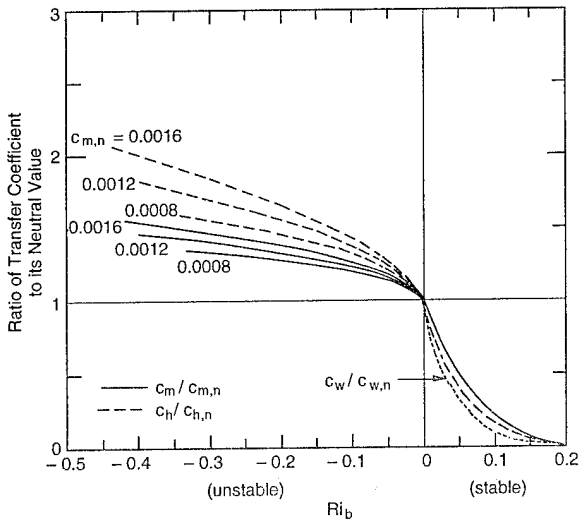

Figure 2. Ratio of bulk transfer coefficient to its neutral value from diabatic profile theory, over a wide range of bulk Richardson numbers. $c_w/c_{w,n}$ is not shown on the unstable side for the fact that it will coincide with $c_h/c_{h,n}$ if $K_w = K_h$ and with $c_m/c_{m,n}$ if $K_w = K_m$ (after Deardorff 1968).

and for the unstable region, the bulk coefficient ratio can be written as

$$\frac{c_m}{c_{m,n}} = 1 + \frac{7}{a}\ln\left(1 - aRi_b\right) \text{ and}$$
$$\frac{c_h}{c_{h,n}} = 1 + \frac{11}{b}\ln\left(1 - bRi_b\right), \tag{46a,b}$$

where $a = 0.83\ (c_{m,n})^{-0.62}$ and $b = 0.25\ (c_{m,n})^{-0.80}$.

Based on the eddy transfer coefficients defined in eq 8, 18, and 19 and the unstable wind, temperature, and specific humidity profiles by

$$\frac{kz}{u_*}\frac{\partial \bar{u}}{\partial z} = \left(1 - \gamma\frac{z}{L}\right)^{-1/4},$$
$$\frac{kzu_*}{-H/\rho c_p}\frac{\partial \bar{T}}{\partial z} = \left(1 - \gamma\frac{z}{L}\right)^{-1/2}, \text{ and} \tag{47a,b,c}$$
$$\frac{kzu_*}{-E/\rho}\frac{\partial \bar{q}}{\partial z} = \left(1 - \gamma\frac{z}{L}\right)^{-n},$$

the ratio of K_h/K_m for the unstable case is

$$\frac{K_h}{K_m} = \left(1 - \gamma\frac{z}{L}\right)^{1/4}, \tag{48}$$

and for the stable case it is

$$\frac{K_h}{K_m} = \frac{\left(1 + \beta_m\frac{z}{L}\right)}{\left(1 + \beta_h\frac{z}{L}\right)}. \tag{49}$$

The ratio of K_w/K_m depends on the exponent n; if $n = 1/4$, then $K_w = K_m$, and if $n = 1/2$, then $K_w/K_m = K_h/K_m$ for the unstable case. For the stable case, the ratio of K_w/K_m as for K_h/K_m can be similarly written as

$$\frac{K_w}{K_m} = \frac{\left(1 + \beta_m\frac{z}{L}\right)}{\left(1 + \beta_h\frac{z}{L}\right)}. \tag{50}$$

Therefore, if β_m, β_h, and β_w are much greater than one, then K_h/K_m and K_w/K_m will approach $\beta_h/\beta_m^2 = 11/49$, corresponding to the value of Ri_c at which the turbulent transfers vanish.

Deardorff (1968) has indicated that $K_m > K_h$ and K_w in the stable case due to the importance of pressure forces in diffusing momentum. If eddies behave somewhat like internal gravity waves, the effect of mixing by molecular processes alone would be rather insignificant, thus $K_m > K_h$ and K_w. Furthermore, the fact that the value of K_h is usually greater than K_w can probably be attributed to the damping of thermal fluctuations by radiative transfer in all directions, and no such mechanism is available to add the mixing of an eddy's excessive water vapor with the surrounding unsaturated air.

C. Empirical wind functions

The turbulent vapor transfer is predominantly a function of wind speed and the vapor pressure gradient and can be expressed in terms of Dalton's relation as

$$E' = f(\overline{U})(e - e_o), \tag{51}$$

where E' is the water vapor transfer expressed as a depth (mm/hr) and $f(\overline{U})$ is a function of the wind speed [mm/(mb • hr)], where E' is positive, the direction of vapor transfer is toward the snow cover (i.e., condensation-forest formation). When E' is negative, it indicates a loss from the snow cover via the process of sublimation and evaporation. The function $f(\overline{U})$ is usually expressed as

$$f(\overline{U}) = a + b\overline{U}\,, \tag{52}$$

where $\overline{U}$ is the product of mean wind speed and time expressed in km, b is an empirical constant expressed in mm/(mb • km • hr), and a is a constant representing the amount of vapor transfer when wind velocity is zero [mm/(mb • hr)]. a is found to be dependent on the time interval being used. The values of both a and b varied a) with the heights at which the wind speed and vapor pressure are measured, b) with the method and the accuracy of snow surface temperature measurement, and c) with the predominating stability conditions and surface roughness of the sites.

For the evaporation of water, a finite value of a results. This reflects evaporation during calm, unstable periods caused by radiative heating of the surface. Since stable conditions usually prevail over a snow cover, the value of a should be zero. Values of a and b can be extrapolated to a constant height of 1 m above the snow surface, i.e.,

$$\frac{\overline{u}_z}{\overline{u}_1} = \frac{\overline{e}_z}{\overline{e}_1} = z^{0.17} \tag{53}$$

where $\overline{u}_z$, $\overline{u}_1$ and $\overline{e}_z$, $\overline{e}_1$ are mean wind speed and vapor pressure at height z and 1 m above the surface, respectively.

The latent heat transfer of evaporation or condensation can be expressed as

$$L_s \rho_w E'' = \frac{L_s \rho_w}{10} E' = \frac{L_s \rho_w}{10} f(\overline{U})(\overline{e} - \overline{e}_o)\,, \tag{54}$$

where E'' is expressed in cm/hr and L_s is the latent heat of sublimation or condensation.

The ratio of sensible heat flux to latent heat flux commonly known as Bowen's ratio, with the assumption of $c_w = c_h$ (also $K_h = K_w$ but that does not assume $K_m \neq K_h$ or K_w) can be written as

$$\frac{Q_h}{Q_e} = \frac{H}{L_s E} = \frac{p c_p \left(\overline{T} - \overline{T}_o\right)}{0.622\, L_s (\overline{e} - \overline{e}_o)}\,. \tag{55}$$

Experimental evidence (Dyer 1967, Pruitt et al. 1971) suggests that the assumption of $K_h = K_w$ is reasonable for all stability conditions. On the other hand, in unstable conditions, K_m is not equal to K_h or K_w (or $c_m \neq c_h$ or c_w). The sensible heat transfer can be written as

$$Q_h = \frac{L_s \rho_w}{10} \gamma f(\overline{U})(\overline{T} - \overline{T}_o)\,, \tag{56}$$

where $\gamma = (p c_p)/0.622\, L_s$ is essentially a constant for a given location.

D. Energy balance method

Since the vertical flux of sensible heat cannot be conveniently measured over long time periods, attempts have been made to measure the other terms in the energy balance equation. The sensible heat flux is found by integrating the energy balance equation to height h (at which the fluxes are measured) plus the fluxes due to radiation q_R, latent heat q_E, and ground conduction q_G (see Lunardini 1981), i.e.,

$$-\rho c_p \overline{w'T'} = -(q_R + q_G + q_E) + c_p \int_0^h \frac{\partial}{\partial x}(\rho \overline{u'T'})dz + c_p \int_0^h \rho \bar{u} \frac{\partial \bar{T}}{\partial x} dz$$

$$+c_p \int_0^h \rho \bar{w} \frac{\partial \bar{T}}{\partial z} dz + c_p \int_0^h \frac{\partial}{\partial z}(\rho \bar{T})dz \tag{57}$$

with the use of the equation of continuity

$$\rho \bar{w} = -\int_0^z \frac{\partial \rho \bar{u}}{\partial x} dz \ .$$

Equation 57 becomes

$$-\rho c_p \overline{w'T'} = -(q_R + q_G + q_E) + c_p \int_0^h \left[\rho \bar{u} \frac{\partial \bar{T}}{\partial z} - \left(\int_0^z \frac{\partial \rho \bar{u}}{\partial x} dz \right) \frac{\partial \bar{T}}{\partial z} \right] dz$$

$$+c_p \int_0^h \frac{\partial}{\partial x}(\rho \overline{u'T'})dz + c_p \int_0^h \frac{\partial}{\partial z}(\rho \bar{T})dz \ . \tag{58}$$

However, the integral terms are not measured in energy balance studies because the contribution from these terms is considered to be rather small in comparison with q_R or q_E, but there is uncertainty whether these terms will be small in comparison with $\rho c_p \overline{w'T'}$, especially if air flow near the test site is obstructed, creating considerable horizontal gradients. Even in the case when there is no obstruction to the air flow, the integral terms are negligible, thus

$$\rho c_p \overline{w'T'} = (q_R + q_E + q_G) \ . \tag{59}$$

The errors in q_R, q_E, and q_G are cumulative and will be lumped together in calculating $\rho c_p \overline{w'T'}$. Since q_R is usually very large, a small error in q_R can thus distort the value of H $(= \rho c_p \overline{w'T'})$ completely. Therefore, the energy balance method cannot provide the credence in evaluating the value of $\rho c_p \overline{w'T'}$.

IV. FUNDAMENTALS IN MEASURING SENSIBLE HEAT FLUX BY CORRELATION TECHNIQUES

As indicated in eq 7, the sensible heat flux is

$$H = \rho c_p \overline{w'T'}. \tag{60}$$

To evaluate the heat flux, H, the covariance of w' and T', i.e., the fluctuating velocity and temperature, has to be measured simultaneously. This requires the use of sophisticated measuring devices and techniques, and the measurement is usually limited to short time spans to have a reasonable approximation of a pseudo-steady-state condition prevailing during the measurement period (this can be accomplished easily by conducting the measurement in artificially controlled conditions such as in a wind tunnel, etc., but not in a constantly changing atmosphere). The correlation technique is the most fundamental one, and the data results from this measurement can be used to evaluate various theories, but we have to be aware that there is great difficulty associated with sampling frequencies, elevations, and site suitability to derive universally applicable expressions. Such types of measurement are not standard operations of meteorological stations, and it is unlikely that they will be in the future.

As we are aware, the turbulent exchange heat fluxes of sensible and latent heat are the most important heat fluxes (the other is radiation heat flux) in the development of the surface energy balance. On a clear day, the radiative flux will obviously predominate. However, during the night or on a cloudy day, the turbulent exchange fluxes will be an essential element affecting the surface energy balance.

Turbulent sensible heat flux has been measured by numerous investigators since the invention of the sonic anemometer and the advances in computer technology since 1965. However, to this author's knowledge, the numerous field experimental results are largely limited to terrains other than snow-covered ground, which presents unique surface characteristics. Because the snow surface serves as the lower boundary, it is generally reported that the numerous turbulent heat flux expressions developed from studies on terrains other than snow will not be applicable to snow-covered ground because the microphysical heat transfer process under extremely stable conditions is still rather poorly understood.

Another phenomenon due to the presence of a snow surface as the lower boundary surface is the validity of the widely accepted concept of the constant flux layer. Although this concept is convenient (because the heat flux is invariant with height), variations of turbulent flux with height have been reported. The discrepancy is attributed to the fact that a term responsible for temperature changes due to the divergence of radiant heat transfer in the thermodynamic energy equation is not included, even though this is considered to be a common micrometeorological practice, especially in the first few meters above the surface. This phenomenon may become more pronounced over snow and melting snow because of their high albedo and the upper-boundary snow temperature of 0°C. Temperature profile anomalies are introduced due to the radiation heating of the air above the snow surface. With the upper-limit snow surface temperature at 0°C, the air over snow is heated to above 0°C, resulting in a stable profile directing heat toward the surface. However, if the air mass is cool, a temperature maximum has been observed in the air layer ~20–50 cm above the surface (De La Casiniere 1974, Halberstam and Schieldge 1981) and about 5 cm above the snow surface by Yen (1993). Above this maximum, the temperature profile is mostly unstable in the case of Halberstam and Schieldge (1981), mostly stable in the work of De La Casiniere (1974), and nearly isothermal for a plot $\overline{T}$ vs. ln Z (Yen 1993) as well as results from Granger (1977) in a linear plot. Under these conditions, not only is the heat flux not a constant with height, but it undergoes a reversal in direction at the level of the raised maximum.

Since an analytical treatment of turbulence research is out of our reach at the present time, the following largely deals with how the field measurement system should be designed and set up to obtain reliable and representative results of universal usage.

A. General problem associated with snow-covered ground

The most prevailing phenomenon of the atmospheric surface layer over snow-covered terrain is the frequent occurrence of very stable conditions. Because of the low thermal conductivity of snow and its high albedo and emissivity, the snow surface can get very cold, especially on clear nights. The snow extracts heat from the air and thus stabilizes the surface layer. Sometimes the surface layer becomes so stable that turbulence ceases completely and any vertical heat transfer is accomplished by much slower molecular transport processes. However, such extremely stable periods do not persist very long because gravity waves or other disturbances distort the stable temperature profile and provide the needed energy for renewed turbulent mixing. These processes are apparently repeated in cyclic fashion and are the key mechanism of the nocturnal boundary layer; they are believed to be an even more intensive occurrence over snow-covered terrain. Consequently, the widely practiced Monin–Obukhov similarity cannot handle such intermittent turbulence.

B. Coverage of frequency intervals

The study of atmospheric turbulence is not a deterministic discipline. Since the air is in random or chaotic motion, we cannot make a single measurement and say "this is the heat flux." In other words, we must deal with the statistics of the turbulence. The key statistic in the study of turbulent heat transfer over snow is the w'–T' covariance $\overline{w'T'}$, w' is the turbulent fluctuation in vertical velocity, T' is the turbulent fluctuating temperature, and the overbar indicates a time average. The sensible heat carried to or from the snow surface is $\rho c_p \overline{w'T'}$, where ρ and c_p are the density and the

specific heat of air, respectively. The simplest way to evaluate the covariance $\overline{w'T'}$ is computed from a time series measurement of w' and T' by

$$\overline{w'T'} = \frac{1}{N}\Sigma w_i' T_i', \tag{61}$$

where N is the number of measurements and w_i' and T_i' are the ith fluctuating vertical velocity and fluctuating temperatures, respectively. However, this rather elementary method will not shed much light on the intricate processes of turbulence. We obtain more information by making the same time series measurements of w' and T' and computing the w' and T' spectra, which are defined in such a way that they yield the variance of w' and T' and the covariance $\overline{w'T'}$, i.e.,

$$\overline{w'^2} = \sigma_{w'}^2 = \int_0^\infty \phi_{w'}(f)\,df \ ,$$

$$\overline{T'^2} = \sigma_{T'}^2 = \int_0^\infty \phi_{T'}(f)\,df \ , \text{ and} \tag{62a,b,c}$$

$$\overline{w'T'} = \int_0^\infty CO_{w'T'}(f)\,df \ ,$$

where f is the turbulent frequency and $\phi_{w'}(f)$, $\phi_{T'}(f)$, and $CO_{w'T'}(f)$ are the spectrum (or spectra density) of w' and T' and the cospectrum of w'–T', respectively. Equation 62 shows not only how the variances and covariance are distributed with respect to spectra and the cospectra but also indicate which eddies accounted for most of the variance or covariance. Kaimal et al. (1972) have established the standard criteria of surface layer spectra. Therefore, based on the collected sonic data we can compute the spectra and cospectra and see if the calculated spectra are in agreement with the characteristics reported by Kaimal and his colleagues. By comparing with the given standard characteristics, we are in a position to learn whether our instruments are operating properly and whether our measuring techniques are correct. If the computed spectra do not possess the well-established spectral shapes already reported, it is certain that either the turbulence measurement or the subsequent analysis or both are not operating properly. Evaluations of $\overline{w'T'}$ from eq 61 will not provide this built-in verification.

The w'–T' spectrum viewed through eq 62c provides guidelines on how to measure $\overline{w'T'}$. Equation 62c indicates that to measure $\overline{w'T'}$ we must sample all frequencies between zero and infinity that contribute to $CO_{w'T'}$. In reality, however, such sampling is neither practical nor possible, because sampling zero frequency would require an infinitely long time series and, on the other hand, sampling frequency to infinity would require an infinitely short sampling interval. The fact is that not all these frequencies contribute to the integral in eq 62c. In dealing with surface-layer turbulence spectra, it is usual to nondimensionalize frequency f by

$$n = f\frac{z}{\bar{u}} \ , \tag{63}$$

where z is the height at which the sonic anemometer is located, and $\bar{u}$ is the mean wind velocity at height z. Kaimal et al. (1972) indicated that the peak value of $CO_{w'T'}$ is usually near $n = 0.1$ and falls off to a value of about 1/10 of its peak value at $n > 7$. Therefore, we usually need only to sample frequencies no higher than $7\ \bar{u}/z$. For $z = 2$ m and $\bar{u} = 2$ m/s, the Nyquist frequency F_{ny} has to be 7 Hz and the actual sampling frequency or digitization rate must be twice F_{ny}, or 14 Hz in this example.

To obtain satisfactory and meaningful values of $\overline{w'T'}$, Wyngaard (1973) suggested that 30 to 60 min of data collection is necessary. For 30 min of data, the lower integration limit of eq 62 is 0.0056 Hz. Even sampling w' and T' for a period of 30 min at a rate of 14 samples per second generates 25,200 data points for each variable. Therefore, to obtain turbulence statistics properly requires collecting a large amount of data.

C. Measurement height determination

In addition to determining the frequency limits needed in the integration of eq 62, we still need to know the height at which the sonic anemometer should be placed. Since a sonic measurement averages w' over a path distance between the sonic arms, it is reasonable to assume that the sonic anemometer should not be placed too near the surface where not only are the velocity and temperature gradients the steepest but the volume of air over which it is averaging would be far from homogeneous; therefore, there is a limitation as to how near the surface the sonic anemometer can be deployed effectively. Kristensen and Fitzjarrald (1984) recommended that the inhomogeneity within the sonic sampling volume is minimal if

$$\frac{z\pi fd}{\overline{u}} < 1 \text{ or } \frac{fz}{\overline{u}} < \frac{z}{2\pi d}, \tag{64}$$

where d is the length of the sonic path. For the example given above, i.e., for $fz/\overline{u} = 7$, then z must be greater than 14 πd if we are to trust the sonic anemometer measurement. The length of d is typically 10 or 20 cm, so the magnitude of z should be at least 4.4 or 8.8 m.

D. Field site selection

The horizontal homogeneity of the area upwind of the measurement site is an important factor in turbulence sampling. To avoid nonrepresentative measurements introduced by internal boundary layers, the area upwind of an instrument must be uniform for a fetch approximately 100 times the measurement height. In the example given in section C above, the upwind fetch must be uniform for a distance of 1400 πd.

V. EXPERIMENTAL

A. Experimental setup

Figure 3 shows the experimental setup. A Campbell Scientific CA27 one-dimensional sonic anemometer (with fine-wire thermocouple) and a hot-film anemometer are linked together and bracketed to the tower post; they can be adjusted to any desired height but are usually set at 2 m above ground level. The sonic heads are set 100 cm away from the tower post. The tip of the hot-film anemometer is positioned at the middle of the sonic path but about 15 cm away from it. The sonic anemometer has an electronic response of 40 Hz, however, the effective limitation is the loss of response to eddies

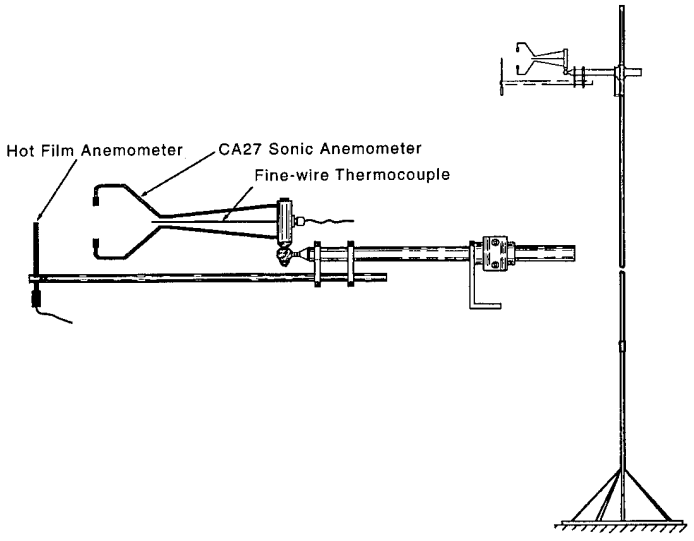

Figure 3. Schematics of experimental setup.

dimensionally smaller than the sonic path length. Since eddy size varies directly with z, the sonic anemometer cannot be used below a certain height. The 10-cm sonic path length reduces the need for the required fetch length. The zero-offset shift in the w signal caused by temperature changes on the sonic transducer precludes the use of a CA27 sonic anemometer (SA) for absolute w measurement. For the same reason, the CA27 SA cannot be used for long-flux averaging periods (i.e., 1 hr). It has been reported that measurements of w' over normal averaging periods compared favorably with values reported by Biltoft and Gaynor (1987) using other SA models. The manufacturer also claimed that the recent model of the CA27 produced less variability in w' than those previously reported by Tanner et al. (1985). The CA27 has a calibration of 1 m/s/V with a range of ±4 m/s.

The tower and its attached SA are so designed that the tower axis is made vertical by adjusting the 4 screws protruding from the corners of the concrete foundation. Ensuring that the CA27 SA is perfectly vertical is accomplished by adjusting the ball-junction so that the air bubble-level on the top of the CA27 SA is centered.

The temperature measurement device is a 13-μm chromel-constantan thermocouple (Model 127, Campbell Scientific, Inc.) with a response of approximately 30 Hz with its signal calibrated to 4°C/V. The absolute air temperature is not measured; instead, the measurement is referenced to the temperature inside the base-mount of the CA27 (Fig. 3). Based on the manufacturer's data, the reference junction has a 20-min interval time constant, which is expected to be adequate for most flux-averaging periods.

Care should be taken to prevent damage to the fine-wire thermocouple, which is extremely fragile. Care also should be taken to avoid any deformation of the silver dish on the acoustical sensors as this can introduce large effects in the wind signal. It is important to note that the transducers employed in the CA27 must not be exposed to wet environments.

The algorithms used by the 21X Micrologger to compute statistical measures on-line require the summation of squares, cross products, and individual values. The covariance of signals x and y is computed from N measurements of x_i and y_i (where superscript i indicates instantaneous value) as

$$\overline{x'y'} = \frac{\Sigma x_i\, y_i}{N} - \frac{\Sigma x_i\, \Sigma y_i}{N^2} ,$$

and the variance of x' is given by

$$\overline{x'^2} = \frac{\Sigma x_i^2}{N} - \left(\frac{\Sigma x_i}{N}\right)^2 .$$

In this investigation, $\overline{x'y'}$ and $\overline{x'^2}$ represent 10-min time averages. For the 10-Hz measurement rate, 6000 samples were needed to generate a single statistical value. In conjunction with using the 21X Micrologger to compute the 20-min variances of temperature, Tanner and Green (1989) clearly show the effect of computation error and found the error is proportional to the number of samples in the averaging period. They reported that as the ratio of the fluctuation to the mean signal $\sigma'_x / \bar{x}$ becomes smaller, the error grows more significant. The variation of relative error, i.e., the ratio of calculated $\sigma_{x'_c}$ to true standard deviation $\sigma_{x'_t}$ as a function of $\sigma_{x'} / \bar{x}$, was calculated by superimposing the sinusoidal fluctuations of the known standard deviation upon different mean values. The results are shown below:

Ratio of $\frac{\sigma'_x}{\bar{x}}$	*Ratio of* $\frac{\sigma_{x'_c}}{\sigma_{x'_t}}$
0.005–0.01	2–4
0.01–0.02	2–1.3
0.02–0.03	1.3–1.1
0.05	<1.05
0.10	1.01

The same reasoning can be applied to the errors in the covariance calculation, i.e., the computational errors become significant if the fluctuations in both signals are small with respect to their means (i.e., $\overline{x'y'}/\overline{xy}$ is small). However, in the measurement of vertical fluxes, the wind signal oscillates around zero (i.e., $\overline{w}$ near zero), thus keeping the ratio large enough to avoid errors in 20-min flux calculations. Based on results reported by Tanner and Green (1989), there were no significant error ratios in fluctuations of T' and w' and its covariance $\overline{w'T'}$.

B. Site description

Theoretically, measurements of surface flux by the eddy-correlation method require an extended upwind surface with reasonably homogeneous flux sources and sinks that is clear of obstacles capable of disrupting the horizontal streamlines from parallel to the surface. These conditions were not met in many of the field measurements reported to date, so the results or empirical formulas developed by the various investigators varied.

In this experiment, the sonic anemometer was installed to sample the northwest prevailing wind direction. However, during the experiment, though we did not record the change of wind direction as a function of time, not only sharp variations in the wind speed but sudden changes in wind direction were frequently observed. Without being equipped with a cut-off device for wind directions other than the desired one (i.e., northwest), the sonic signals gathered are bound to be rather complex; they are composed of effects due not only to variations of wind speed and direction, but to obstacles causing the upwind flow to be neither homogeneous nor parallel to the surface.

As indicated by Yen (1993), a considerable amount of time and effort was directed to securing a test site that was logistically as well as economically feasible for micrometeorological measurements. Even after a concerted effort, however, we still were unable to select a site to meet the requirements outlined above in A, Experimental Setup. A small (about 8 m × 8 m) site located behind CRREL's main building was finally chosen. The site is elevated on three sides and bordered on one side with a similar but smaller rectangular cavity. All around the site all sorts of obstacles, such as trees, buildings, a hut, and plants, offer resistance to air flow and create extra air turbulence that contrasts with a normally homogeneous field that has a large and smooth upwind fetch. Though we knew from the onset that the results obtained from this non-ideal site would not provide any universal usage, it did enable the researcher to gain some experience and insight in microphysical measurements and provided a basis for comparison with other reported results measured under more or less similar conditions.

Along with the sonic measurement, an accompanying measurement of the air temperature (near the sonic measurement) at various heights (up to 1.29 m) was also carried out. Its aim was to verify the reported results that there is a temperature inversion near the surface layer. A Campbell CR7 data logger was programmed to take the eight thermocouple readings at sampling rates of 30 s, 1, or 2 min, with the selection of data averaging time ranging from 1, 10, 20, 30, or 60 min.

VI. RESULTS AND DISCUSSION

Sonic turbulent heat flux measurements commenced in May 1991 and continued for as long as meteorological conditions permitted (it is not feasible to collect data on very windy days or when it is raining or snowing). Over the period 1991–1992, 46 sets of flux data were collected. Due to the lack of snowfall during the winter, only 10 sets of the data were taken over either a shallow snow layer, a thin ice layer, or a spotty (or patchy) snow cover.

In early April 1992, due to construction activities occurring near the test site and problems with the meteorological data-gathering facilities for wind-speed direction and net radiation data, this series of tests was terminated. The test tower and the other associated measuring devices were moved to the Geophysical Sciences Branch field test site in front of the Frost Effects Research Facility in August 1992.

A. Collection and analysis of data

Sonic data were collected with a 21X Micrologger based on a sampling rate of 10 per second and an averaging period of 10 minutes (mostly). Six thousand readings were used to evaluate each data point shown in the following figures.

Instantaneous vertical wind speed, fluctuating temperatures, and the horizontal wind speed measured by the hot-film anemometer were collected at 10 samples per second but were discarded after the 10-minute average values were evaluated. The micrologger was programmed to receive and compute the reference temperature; the fine thermocouple reading at the measurement height; the average vertical wind speed $\overline{w}$; the mean of the fluctuating temperature $\overline{T}$; the mean of the horizontal wind speed $\overline{u}$; the standard deviations of the vertical wind speed $\sigma_{w'}\left(=\sqrt{\overline{w'^2}}\right)$, the vertical temperature $\sigma_{T'}\left(=\sqrt{\overline{T'^2}}\right)$, and the horizontal wind speed $\sigma_{u'}\left(=\sqrt{\overline{u'^2}}\right)$; and the covariances of $\overline{w'T'}$ and $\overline{u'w'}$.

Two typical sets of collected and computed values are shown in Table 1 and Table 2. Table 1 shows file number 9107101440, which covered a period of about 8 hr with 10-min data average output. Table 2 shows file number 9107160815, which covered a period from 19:40 p.m. EST on 15 July, 1991, to 8:10 a.m. the next morning. The first and last 10-minute data were not used for subsequent analysis, to ensure elimination of unsteady effects. Table 1b and Table 2b show the friction velocity u_*, the Obukhov length L, the ratio of $\sigma_{w'}/u_*$, the stability criterion z/L, and T_a, the mean absolute air temperature. The values of $\overline{T}$, $\overline{u}$, $\sigma_{w'}$, $\overline{w'T'}$, and $\overline{u'w'}$ are used to define the values of u_*, L, and $\sigma_{w'}/u_*$. Looking at Table 1b, and based on the values of z/L, the atmosphere was clearly unstable during the entire measurement period. The mean wind speed $\overline{u}$ varied from a minimum of 1.46 to a maximum of 4.31 m/s. Since we did not have the means to determine and record the wind direction during the measurements, the random obstacles surrounding the test site caused a great variation of turbulence characteristics affecting the value of $\sigma_{w'}\left(=\sqrt{\overline{w'^2}}\right)$, which is a measure of the intensity of the vertical fluctuating velocity. Indirectly it also affected the sensible heat flux (i.e., $\rho c_p \overline{w'T'}$ and the value of u_*, which is calculated from $\left(-\overline{u'w'}\right)^{1/2}$.

Contrary to the results listed in Table 1b, the data shown in Table 2b are rather erratic. Since this set of data was collected over a period from the evening to the next morning, the atmosphere was in either a stable or a slightly unstable state. This phenomenon was evidenced by the values of $\overline{w'T'}$, which are mostly near zero and associated with alternate positive and negative signs (a negative sign indicates the heat is extracted from the air and the atmosphere is stable). In cases when $\overline{u'w'}$ had positive values, the data were eliminated along with the cases when the value of L was 0, infinity, or a ratio of 0/0. It should also be noted that the values of $\overline{u}, \sigma_{w'}, \sigma_{u'}$ along with $\overline{w'T'}$ and $\overline{u'w'}$, are much smaller in magnitude when compared with those shown in Table 1b. This is because the atmosphere is near neutral stability, and the transports of heat and momentum are mostly dominated by molecular processes.

In all, 47 sets of sonic heat flux measurements were made over the period from May 1991 to April 1992. Most of the measurements were conducted from middle (or early) morning and ended in late afternoon, depending on the weather conditions. Since the sonic anemometer cannot be used under wet conditions, no tests were conducted on snowy, rainy, or windy days to ensure that no damage would be done to the sonic probe and the fine-hair thermocouple.

The following figures show the variation of friction velocity u_* and standard deviations σ'_w and σ'_u with mean wind speed $\overline{u}_{2m}$, as well as the variations of σ'_w and σ'_u with u_* (to avoid overcrowding the data points and the difficulty in using different notations for different sets of data). Only six sets of data (91061345, 9106271405, 9107011334, 9107031408, 9107101440, and 9107301320) were plotted and only full dot notation was used. These plots were compared with those reported by Kai (1982) in his study of statistical characteristics of turbulence and the budget of turbulent energy in the surface boundary layer. Kai's measurement was conducted at a site that is circular in shape with a radius of 80 m and covered by 0.5-m-tall grass. The 30-m tower was erected

Table 1. Data from test 9107101440, taken in unstable conditions.

a. Measured data

Test period	Time of day	Panel temperature (°C)	Air temperature (°C)	$\overline{w}$ (m/s)	$\overline{T}$ (°C)	$\overline{u}_{2m}$ (m/s)	$\sigma_{w'}$ (m/s)	$\sigma_{T'}$ (°C)	$\sigma_{u'}$ (m/s)	$\overline{w'T'}$ (m °C/s)	$\overline{u'w'}$ (m^2/s^2)
1	0850	15.93	16.83	0.124	–3.325	2.937	0.340	0.490	0.018	0.083	0.000
2	0900	16.92	17.20	0.098	–3.273	2.628	0.322	0.551	0.670	0.087	–0.025
3	0910	18.26	17.70	0.111	–3.616	1.936	0.313	0.615	0.541	0.091	–0.041
4	0920	19.92	18.07	0.075	–3.906	1.546	0.276	0.664	0.631	0.086	–0.055
5	0930	20.70	18.31	0.052	–4.160	2.016	0.287	0.587	0.624	0.083	–0.036
6	0940	20.53	19.02	0.113	–3.971	1.457	0.253	0.677	0.669	0.098	–0.038
7	0950	20.76	19.62	0.122	–4.426	1.722	0.293	0.722	0.698	0.089	–0.028
8	1000	21.06	19.96	0.052	–4.170	2.161	0.314	0.773	0.572	0.112	–0.045
9	1010	21.51	20.66	0.097	–3.819	1.795	0.295	0.679	0.643	0.099	–0.027
10	1020	22.05	21.01	0.120	–4.070	1.794	0.339	0.718	0.54	0.118	–0.017
11	1030	22.52	21.53	0.133	–3.787	1.728	0.299	0.698	0.672	0.098	–0.010
12	1040	23.10	22.08	0.069	–3.927	2.165	0.320	0.735	0.585	0.111	–0.050
13	1050	23.61	22.49	0.109	–3.860	1.638	0.326	0.844	0.684	0.134	–0.060
14	1100	23.99	22.11	0.094	–4.283	1.883	0.307	0.886	0.848	0.120	–0.068
15	1110	24.40	23.13	0.106	–3.869	1.552	0.396	0.828	0.853	0.134	–0.056
16	1120	25.11	23.27	0.144	–4.335	2.984	0.476	0.934	1.222	0.136	–0.097
17	1130	25.37	23.42	0.122	–2.521	4.306	0.714	0.584	1.418	0.143	–0.194
18	1140	25.68	23.98	0.056	–2.205	3.477	0.634	0.697	1.383	0.157	–0.176
19	1150	26.16	23.99	0.121	–2.767	3.446	0.634	0.628	1.250	0.135	–0.123
20	1200	26.58	24.54	0.077	–2.474	3.117	0.591	0.762	1.363	0.198	–0.168
21	1210	26.99	24.23	0.000	–2.876	4.056	0.699	0.693	1.450	0.193	–0.283
22	1220	27.57	24.38	0.137	–2.031	3.281	0.609	0.779	1.329	0.187	–0.098
23	1230	28.00	24.33	0.137	–2.856	3.036	0.490	0.831	1.092	0.166	–0.108
24	1240	28.29	24.26	0.128	–2.904	3.407	0.569	0.709	1.265	0.138	–0.180
25	1250	28.38	24.37	0.121	–2.050	2.617	0.474	0.840	1.05	0.155	–0.094
26	1300	28.51	24.74	0.063	–2.168	2.981	0.507	0.911	1.185	0.214	–0.147
27	1310	28.60	24.33	0.092	–2.300	3.057	0.530	0.921	1.181	0.103	–0.141
28	1320	28.66	24.70	0.069	–2.206	2.162	0.437	0.762	0.959	0.123	–0.020
29	1330	28.61	24.47	–0.035	–2.081	2.554	0.654	0.862	1.212	0.213	–0.217
30	1340	28.92	25.09	0.055	–2.342	3.455	0.614	0.922	1.288	0.233	–0.151
31	1350	29.36	24.85	0.077	–2.803	3.992	0.633	0.853	1.529	0.233	–0.249
32	1400	29.49	24.47	0.006	–2.744	3.064	0.475	0.739	1.384	0.105	–0.107
33	1410	29.80	25.33	0.097	–0.693	2.568	0.444	0.995	1.122	0.182	–0.110
34	1420	30.30	25.07	9.126	–3.566	2.411	0.428	0.851	0.966	0.147	–0.116
35	1430	30.40	24.99	0.137	–3.085	3.282	0.15	0.676	1.373	0.107	–0.070

b. Computed data.

Test period	u_* (m/s)	L (m)	$\frac{\sigma_{w'}}{u_*}$	$\frac{z}{L}$	T_a (K)
2	0.16	–3.36	2.04	–0.59	290.20
3	0.20	–6.77	1.55	–0.30	290.70
4	0.23	–11.14	1.18	–0.18	291.07
5	0.19	–6.12	1.51	–0.33	291.31
6	0.19	–5.63	1.30	–0.36	292.02
7	0.17	–3.93	1.75	–0.51	292.62
8	0.21	–6.37	1.48	–0.31	292.96
9	0.16	–3.36	1.80	–0.60	293.66
10	0.13	–1.41	2.60	–1.42	294.01
11	0.10	–0.77	2.99	–2.61	294.53
12	0.22	–7.58	1.43	–0.26	295.08
13	0.24	–8.27	1.33	–0.24	295.49
14	0.26	–11.12	1.18	–0.18	295.11
15	0.24	–7.47	1.67	–0.27	296.13
16	0.31	–16.79	1.53	–0.12	296.27
17	0.44	–45.188	1.62	–0.04	296.42
18	0.42	–35.63	1.51	–0.06	296.98
19	0.35	–24.21	1.81	–0.08	296.98

Table 1b (cont'd).

Test period	u_* *(m/s)*	L *(m)*	$\frac{\sigma_{w'}}{u_*}$	$\frac{z}{L}$	T_a *(K)*
20	0.41	–26.40	1.44	–0.08	297.54
21	0.50	–50.00	1.39	–0.04	297.23
22	0.31	–12.45	1.95	–0.16	297.38
23	0.33	–16.22	1.49	–0.12	297.33
24	0.42	–41.96	1.34	–0.05	297.26
25	0.31	–14.56	1.53	–0.14	297.37
26	0.38	–20.00	1.32	–0.10	297.74
27	0.38	–38.97	1.41	–0.05	297.22
28	0.14	–1.75	3.09	–1.15	297.70
29	0.47	–36.01	1.40	–0.06	297.47
30	0.39	–19.15	1.58	–0.10	298.09
31	0.50	–50.49	1.27	–0.04	297.09
32	0.33	–25.30	1.45	–0.08	297.47
33	0.33	–15.26	1.34	–0.13	298.33
34	0.34	–20.44	1.26	–0.10	298.07

Table 2. Data from test 9107160815, taken in conditions of near-neutral stability.

a. Measured data

Test period	*Time of day*	*Panel temperature (°C)*	*Air temperature (°C)*	$\overline{w}$ *(m/s)*	$\overline{T}$ *(°C)*	$\overline{u}_{2m}$ *(m/s)*	$\sigma_{w'}$ *(m/s)*	$\sigma_{T'}$ *(°C)*	$\sigma_{u'}$ *(m/s)*	$\overline{w'T'}$ *(m °C/s)*	$\overline{u'w'}$ *(m^2/s^2)*
1	1940	29.81	25.93	0.080	–4.274	0.619	0.097	0.386	0.112	0.008	–0.002
2	1950	29.40	24.90	0.090	–4.984	0.618	0.094	0.338	0.136	0.000	0.000
3	2000	29.77	23.77	0.098	–4.714	0.555	0.072	0.27	0.226	0.001	–0.003
4	2010	29.85	23.45	0.116	–4.578	0.378	0.049	0.144	0.090	0.000	0.000
5	2020	29.64	22.32	0.130	–4.180	0.373	0.045	0.435	0.112	–0.004	–0.001
6	2030	29.20	21.30	0.131	–3.193	0.450	0.051	0.344	0.168	–0.004	0.000
7	2040	28.62	20.59	0.150	–2.432	0.413	0.076	0.252	0.159	–0.002	0.000
8	2050	27.96	0.03	0.151	–1.83	0.370	0.094	0.330	0.179	0.006	0.001
9	2100	27.30	19.68	0.135	–1.074	0.434	0.064	0.409	0.202	0.001	0.000
10	2110	26.65	19.34	0.173	–0.956	0.639	0.065	0.307	0.105	0.000	0.000
11	2120	26.02	19.12	0.138	–0.452	0.734	0.066	0.204	0.111	–0.004	0.000
12	2130	25.43	18.73	0.158	–0.349	0.557	0.038	0.187	0.128	0.000	0.000
13	2140	24.88	18.29	0.160	–0.381	0.547	0.058	0.305	0.206	–0.001	0.000
14	2150	24.35	18.23	0.164	–0.222	0.623	0.098	0.349	0.147	–0.007	0.000
15	2200	23.83	17.61	0.161	–0.238	0.417	0.039	0.31	0.103	–0.001	0.000
16	2210	23.34	17.38	0.212	–0.240	0.549	0.333	0.196	0.141	–0.016	–0.003
17	2220	22.87	17.15	0.171	–0.076	0.507	0.059	0.119	0.105	0.000	0.000
18	2230	22.42	16.85	0.143	–0.124	0.534	0.048	0.135	0.173	0.000	0.000
19	2240	2.00	16.64	0.176	0.040	0.459	0.051	0.267	0.199	0.002	–0.001
20	2250	21.59	16.50	0.167	0.010	0.556	0.054	0.226	0.116	–0.002	–0.001
21	2300	21.18	16.04	0.171	–0.244	0.417	0.062	0.109	0.182	0.000	–0.001
22	2310	20.79	15.88	0.157	0.016	0.457	0.058	0.113	0.153	0.000	0.000
23	2320	20.44	15.69	0.173	0.010	0.450	0.053	0.167	0.150	–0.002	–0.002
24	2330	20.11	15.71	0.168	0.283	0.484	0.097	0.223	0.160	–0.004	–0.004
25	2340	19.77	15.59	0.158	0.082	0.480	0.073	0.129	0.153	–0.001	0.000
26	2350	19.45	15.22	0.163	0.011	0.508	0.078	0.200	0.194	–0.007	–0.001
27	0000	19.13	15.08	0.143	–0.013	0.805	0.085	0.128	0.081	0.000	–0.002
28	0010	18.84	14.93	0.167	0.013	0.568	0.095	0.226	0.200	0.001	–0.005
29	0020	18.56	14.58	0.185	0.122	0.304	0.049	0.178	0.101	0.000	0.000
30	0030	18.26	14.39	0.184	0.024	0.382	0.058	0.121	0.176	0.000	0.001
31	0040	17.97	14.20	0.195	0.171	0.290	0.036	0.137	0.078	0.001	0.000
32	0050	17.68	14.21	0.174	0.244	0.368	0.039	0.194	0.127	0.000	0.000
33	0100	17.40	13.95	0.196	0.193	0.371	0.040	0.141	0.158	0.000	0.000
34	0110	17.40	13.91	0.180	0.219	0.496	0.061	0.141	0.151	0.000	0.000
35	0120	16.90	13.84	0.184	0.183	0.405	0.054	0.192	0.118	0.002	0.000
36	0130	16.67	13.64	0.184	0.205	0.333	0.033	0.065	0.095	0.000	0.000

Table 2 (cont'd). Data from test 9107160815, taken in conditions of near-neutral stability.

a. Measured data (cont'd)

Test period	*Time of day*	*Panel temperature (°C)*	*Air temperature (°C)*	$\overline{w}$ *(m/s)*	$\overline{T}$ *(°C)*	$\overline{u}_{2m}$ *(m/s)*	$\sigma_{w'}$ *(m/s)*	$\sigma_{T'}$ *(°C)*	$\sigma_{u'}$ *(m/s)*	$\overline{w'T'}$ *(m °C/s)*	$\overline{u'w'}$ *(m^2/s^2)*
37	0140	16.43	13.66	0.187	0.332	0.340	0.032	0.188	0.075	0.000	0.000
38	0150	16.21	13.44	0.208	0.206	0.503	0.051	0.134	0.122	0.000	0.000
39	0200	16.01	13.27	0.197	0.305	0.417	0.066	0.176	0.078	–0.002	0.000
40	0210	15.82	13.28	0.185	0.296	0.460	0.046	0.144	0.099	0.000	0.000
41	0220	15.64	12.96	0.188	0.279	0.237	0.036	0.173	0.078	0.000	0.000
42	0230	15.47	13.11	0.189	0.514	0.506	0.044	0.140	0.073	–0.001	0.000
43	0240	15.30	12.99	0.20	0.373	0.492	0.041	0.095	0.075	0.000	0.000
44	0250	15.13	12.96	0.180	0.581	0.496	0.090	0.266	0.176	–0.007	0.000
45	0300	14.97	12.81	0.193	0.252	0.396	0.052	0.210	0.230	–0.002	0.000
46	0310	14.81	12.53	0.172	0.478	0.036	0.036	0.136	0.094	0.000	0.000
47	0320	14.64	12.55	0.207	0.306	0.544	0.053	0.105	0.148	0.000	0.000
48	0330	14.49	12.43	0.192	0.272	0.840	0.086	0.134	0.161	0.000	–0.006
49	0340	14.38	12.53	0.191	0.400	0.718	0.089	0.099	0.087	–0.002	–0.002
50	0350	14.27	12.61	0.180	0.456	0.698	0.086	0.090	0.102	–0.002	–0.002
51	0400	14.19	12.70	0.204	0.490	0.710	0.091	0.105	0.092	–0.003	0.000
52	0410	14.13	12.59	0.181	0.406	0.599	0.079	0.076	0.157	–0.002	–0.002
53	0420	14.04	12.24	0.204	0.161	0.473	0.054	0.160	0.199	0.000	0.005
54	0430	13.91	11.94	0.192	0.242	0.278	0.043	0.203	0.087	–0.003	–0.001
55	0440	13.75	12.08	0.205	0.472	0.409	0.075	0.148	0.181	–0.002	–0.003
56	0450	13.59	11.99	0.205	0.389	0.306	0.043	0.163	0.141	0.000	–0.001
57	0500	13.47	11.72	0.209	0.353	0.603	0.065	0.135	0.179	–0.002	–0.001
58	0510	13.36	11.85	0.210	0.561	0.431	0.080	0.155	0.162	0.000	–0.003
59	0520	13.30	12.15	0.203	0.565	0.523	0.089	0.068	0.210	0.000	–0.007
60	0530	13.34	12.38	0.170	0.285	1.012	0.117	0.174	0.308	0.003	–0.007
61	0540	13.43	12.31	0.158	0.050	0.861	0.112	0.062	0.209	0.002	–0.002
62	0550	13.52	12.33	0.215	0.012	0.597	0.107	0.075	0.200	0.003	–0.006
63	0600	13.60	12.27	0.195	–0.116	0.492	0.099	0.092	0.240	0.004	–0.006
64	0610	13.67	12.20	0.161	–0.212	0.823	0.149	0.091	0.195	0.007	–0.010
65	0620	13.72	12.12	0.187	–0.226	0.860	0.141	0.112	0.213	0.007	0.000
66	0630	13.79	12.25	0.190	–0.123	0.634	0.106	0.091	0.134	0.005	–0.002
67	0640	13.85	12.38	0.172	–0.207	0.783	0.123	0.135	0.220	0.007	–0.002
68	0650	13.93	12.38	0.190	–0.341	0.682	0.109	0.145	0.315	0.008	–0.008
69	0700	14.03	12.52	0.185	–0.448	0.749	0.143	0.230	0.223	0.020	–0.009
70	0710	14.15	12.52	0.184	–0.730	0.646	0.132	0.177	0.158	0.004	–0.004
71	0720	14.30	12.70	0.164	–0.862	0.698	0.158	0.218	0.211	0.019	–0.002
72	0730	14.48	12.77	0.166	–1.179	0.745	0.142	0.232	0.245	0.013	–0.002
73	0740	14.67	12.82	0.199	–1.494	0.868	0.165	0.214	0.244	0.017	–0.005
74	0750	14.89	13.06	0.208	–1.808	1.053	0.153	0.355	0.253	0.031	–0.013
75	0800	15.17	13.23	0.201	–2.452	1.387	0.185	0.380	0.01	0.033	–0.006
76	0810	15.50	13.62	0.183	–3.089	1.022	0.168	0.579	0.407	0.044	–0.007

b. Computed data.

Test period	u_* *(m/s)*	L *(m)*	$\frac{\sigma_{w'}}{u_*}$	$\frac{z}{L}$	T_a *(K)*
2	inconsistency:	L=0/0			
3	0.05	–12.44	1.31	–0.16	296.77
4	inconsistency:	L=0/0			
5	0.03	0.60	1.42	3.36	295.32
6	inconsistency:	L=0			
7	inconsistency:	L=0/0			
8	error: $\overline{u'w'}$ is positive.				
9	inconsistency:	L=0			
10	inconsistency:	L=0			
11	inconsistency:	L=0/0			
12	inconsistency:	L=0			
13	inconsistency:	L=0/0			

Table 2b (cont'd).

Test period	u_* *(m/s)*	L *(m)*	$\frac{\sigma_{w'}}{u_*}$	$\frac{z}{L}$	T_a *(K)*
14	0.03	0.34	3.10	5.96	291.23
15	inconsistency:	L=0			
16	0.05	0.76	6.08	2.63	290.38
17	inconsistency:	L=0/0			
18	0.04	inf.	1.07	0.000	289.85
19	0.03	−1.17	1.61	−1.71	289.64
20	0.03	1.17	1.71	1.71	289.50
21	0.03	inf.	1.96	0.000	289.04
22	inconsistency:	L=0/0			
23	0.04	3.29	1.19	0.61	288.69
24	0.06	4.66	1.53	0.43	288.71
25	inconsistency:	L=0			
26	0.03	0.33	2.47	6.02	288.22
27	0.04	inf.	1.90	0.000	299.08
28	0.07	−25.97	1.34	−0.08	287.93
29	inconsistency:	L=0/0			
30	error: $\overline{u'w'}$ is positive.				
31	inconsistency:	L=0			
32	inconsistency:	L=0/0			
33	inconsistency:	L=0/0			
34	inconsistency:	L=0/0			
35	inconsistency:	L=0			
36	inconsistency:	L=0/0			
37	inconsistency:	L=0/0			
38	inconsistency:	L=0/0			
39	inconsistency:	L=0			
40	inconsistency:	L=0/0			
41	inconsistency:	L=0/0			
42	inconsistency:	L=0			
43	inconsistency:	L=0/0			
44	inconsistency:	L=0			
45	inconsistency:	L=0			
46	inconsistency:	L=0/0			
47	inconsistency:	L=0/0			
48	0.08	inf.	1.11	0.000	285.43
49	0.04	3.26	1.99	0.61	285.53
50	0.04	6.52	1.92	0.31	285.61
51	inconsistency:	L=0			
52	0.04	3.26	1.77	0.61	285.59
53	error: $\overline{u'w'}$ is positive.				
54	0.03	0.77	1.36	2.61	284.94
55	0.05	5.97	1.37	0.33	285.08
56	0.03	inf.	1.36	0.000	284.99
57	0.03	1.15	2.06	1.74	284.72
58	0.05	inf.	1.46	0.000	284.85
59	0.08	inf.	1.06	0.000	285.15
60	0.08	−14.21	1.40	−0.14	285.38
61	0.04	−3.25	2.50	−0.61	285.31
62	0.08	−11.28	1.38	−0.18	285.33
63	0.08	−8.46	1.28	−0.24	285.27
64	0.10	−10.39	1.49	−0.19	285.20
65	inconsistency:	L=0			
66	0.04	−1.30	2.37	−1.54	28.25
67	0.04	−0.93	2.75	−2.15	285.38
68	0.09	−6.51	1.22	−0.31	285.38
69	0.09	−3.11	1.51	−0.64	285.52
70	0.06	−1.32	2.09	−1.52	285.52
71	0.04	−0.34	3.53	−5.83	285.70
72	0.04	−0.50	3.18	−3.99	285.77
73	0.07	−1.52	2.33	−1.32	285.82
75	0.13	−4.48	1.46	−0.45	286.23

at the center with four (3-component) sonic anemometers and resistance thermometers installed at 1.6, 4.3, 12.3, and 29.5 m above the ground. The booms for the sonic anemometers and the resistance thermometers extended 2.0 m southeast and northeast, respectively.

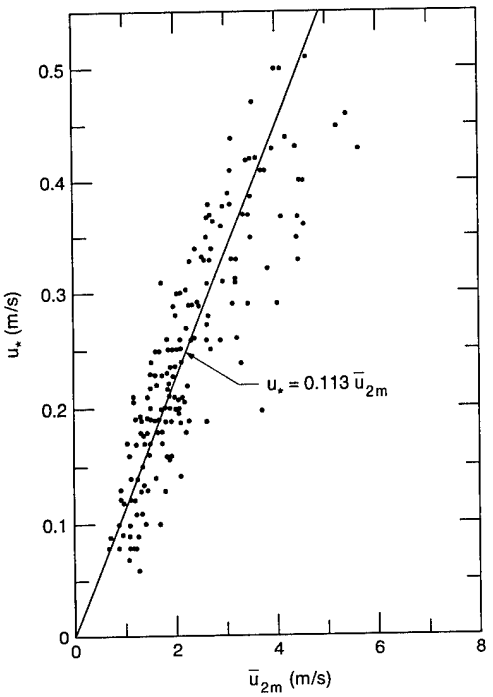

Figure 4. Friction velocity u_* *as a function of mean wind speed at* $\bar{u}_{2m}$.

Figure 4 shows the relation between u_* and $\bar{u}_{2m}$. For six sets of data taken during the months of June and July 1991, a simple linear relationship can be expressed as

$$u_* = 0.113\,\bar{u}_{2m}\ , \tag{65}$$

which is found to be identical to the average relationship developed by Kai (1982), i.e., $u_* = 0.11\bar{u}$ (in Kai's test there are four sonic anemometers, so there is one linear relation for each level: $u_* = 0.10\bar{u}$ at 1.6 m, $u_* = 0.12\bar{u}$ at 4.3 m, $u_* = 0.12\bar{u}$ at 12.3 m, and $u_* = 0.09\bar{u}$ at 29.5 m.

Figure 5a shows the standard deviation $\sigma_{w'}$, representing the turbulent fluctuation in the vertical direction, as a function of the mean wind speed. As in Figure 4, the relationship can be linearly represented by

$$\sigma_{w'} = 0.16\,\bar{u}_{2m}\ . \tag{66}$$

It shows that $\sigma_{w'}$ increases with $\bar{u}_{2m}$. It was surprising to note that an identical relation was developed by Kai (1982) from test results gathered from a much more homogeneous field (i.e.,

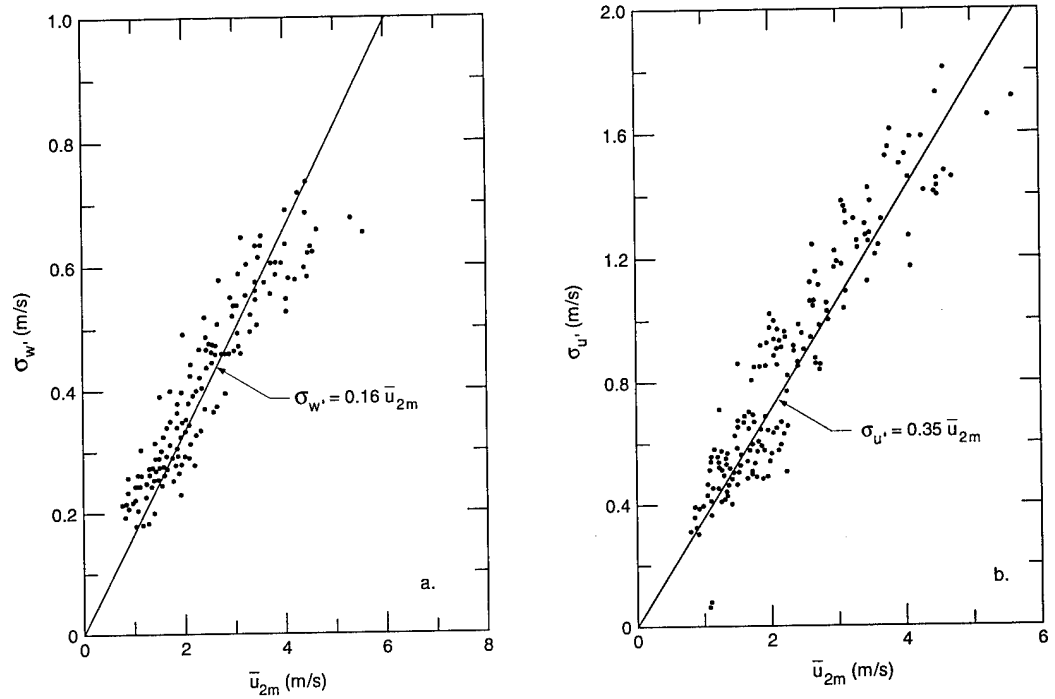

Figure 5. Standard deviations $\sigma_{w'}$ *(a) and* $\sigma_{u'}$ *(b) as a function of mean wind speed at* $\bar{u}_{2m}$.

$\sigma_{w'} = 0.16\,\bar{u}$; this relationship is also developed from measurements at four different heights, as indicated earlier). Kai further noted that the ratio of $\sigma_{w'}/\bar{u}$ at the highest level (i.e., z = 29.5 m) is slightly lower than those at levels z = 1.6 to 12.3 m.

Figure 5b shows the relation of $\sigma_{u'}$ vs. $\bar{u}_{2m}$ (the value of $\sigma_{u'}$ is generated not from the unidirectional sonic anemometer but from the hot-film anemometer). A linear relationship of

$$\sigma_{u'} = 0.35\,\bar{u}_{2m} \tag{67}$$

represents the data rather well, but the increase of $\sigma_{u'}$ with $\bar{u}_{2m}$ is about 60% higher than the one reported by Kai (i.e., $\sigma_{u'} = 0.25\,\bar{u}$). This discrepancy might be due to the fact that $\sigma_{u'}$ was measured from a hot-film anemometer (which is not as sensitive as the sonic anemometer) and the test site is much less homogeneous than the one Kai used. Kai also points out that there seems to be smaller scatter in $\sigma_{w'}$ than in the horizontal components $\sigma_{u'}$ and $\sigma_{v'}$.

Figure 6a shows the variation of $\sigma_{u'}$ (the horizontal component of the turbulent fluctuation) with u_* and can be represented by

$$\sigma_{u'} = 3.7\,u_*. \tag{68}$$

Like the case of $\sigma_{u'}$ vs. $\bar{u}_{2m}$, this relation has a higher coefficient than the one presented by Kai (i.e., $\sigma_{u'} = 2.53\,u_*$). Figure 6b shows the variation of $\sigma_{w'}$ with u_* and can be represented by

$$\sigma_{w'} = 1.6\,u_*\,, \tag{69}$$

which is nearly identical to the relation presented by Kai (i.e., $\sigma_{w'} = 1.58\,u_*$) covering the measurement at four levels. As noted in Kai's paper, in both plots of $\sigma_{w'}$ vs. u_* or $\bar{u}_{2m}$ and $\sigma_{u'}$ vs. u_* or $\bar{u}_{2m}$, the horizontal components $\sigma_{u'}$ and $\sigma_{v'}$ (in Kai's case) have a greater scatter than the vertical component $\sigma_{w'}$. The ratio of $\sigma_{u'}/\sigma_{w'}$ is about 2.33 in this study as compared with Kai's of 1.60. The higher ratio of $\sigma_{u'}/\sigma_{w'}$ can be attributed to the inhomogeneity of the test site (the upwind fetch length requirement was never met).

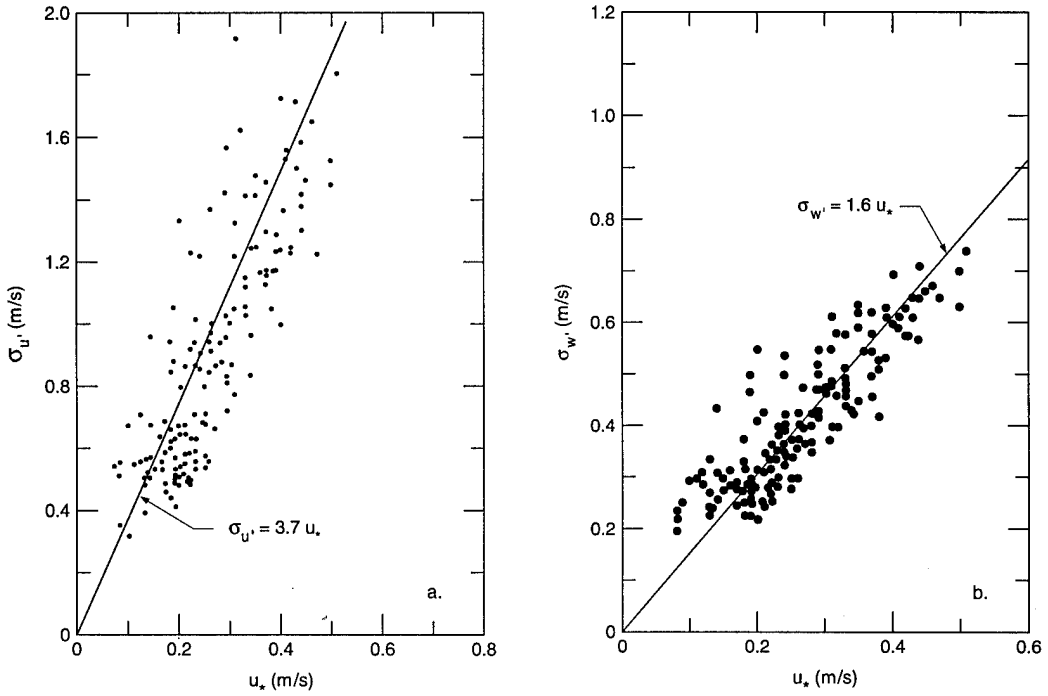

Figure 6. Standard deviations $\sigma_{u'}$ (a) and $\sigma_{w'}$ (b) as a function of friction velocity u_*.

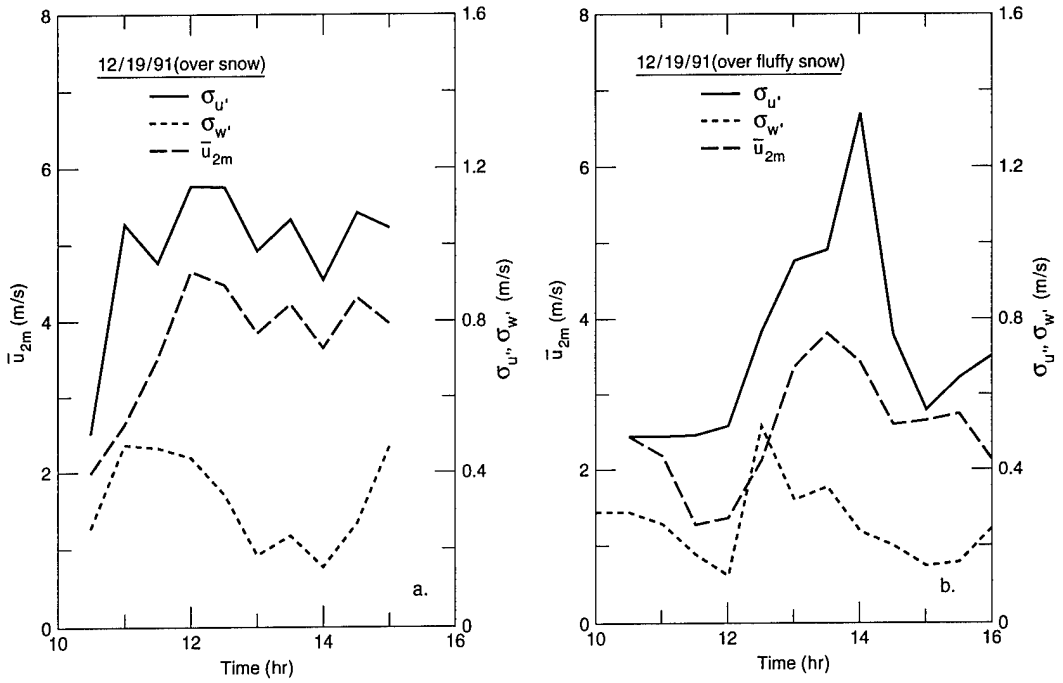

Figure 7. Variation of $\sigma_{u'}$, $\sigma_{w'}$ and $\bar{u}_{2m}$ with time (a) over snow and (b) over fluffy snow.

Figures 7a and 7b respectively show the variation of $\bar{u}_{2m}$, $\sigma_{u'}$, and $\sigma_{w'}$ as functions of time over snow with different structures. There seemed to be no one-to-one correspondence between the turbulence intensity of $\sigma_{u'}$ and $\sigma_{w'}$, i.e., when $\sigma_{u'}$ is at maximum $\sigma_{w'}$ is not. The variation of $\bar{u}_{2m}$ does resemble $\sigma_{u'}$ more than $\sigma_{w'}$. It can be noted that in both cases the peak value of $\sigma_{w'}$ was reached before the highest value of $\bar{u}_{2m}$ occurred. This phenomenon may be attributed to the rapid warming of the surface air layer and its subsequent rising, which introduces added upward natural convection. In both cases, the ratio of $\sigma_{u'}/\sigma_{w'}$ varies from about 1.5 to 5.5.

Figure 8 shows the relation between the covariance $\overline{w'T'}$ and the ratio of $\bar{u}_{2m}/u_*$, which covered eight sets of data taken over a field of grass that was about 3 cm high. The covariance $\overline{w'T'}$ can be fairly represented by

$$\overline{w'T'} = 0.212 - 0.013\frac{\bar{u}_{2m}}{u_*} \quad . \tag{70}$$

It indicates that as u_{2m}/u_* increases, $\overline{w'T'}$ decreases. In other words, for the same value of $\bar{u}_{2m}$ but with u_* increasing, there will be larger values of $\overline{w'T'}$. The larger the value of u_*, the more momentum transfer there is. For a value of u_{2m}/u_* equal to ~16.3, if the above relation holds, the value of $\overline{w'T'}$ approaches zero.

Figure 9 shows the variation of $\overline{w'T'}$ with $\bar{u}_{2m}$. This figure covers the period from May to July 1991 and consists of nine sets of data. Though the graph shows a greater scatter (which is not unusual for micrometeorological measurements), there is a concrete trend that $\overline{w'T'}$ increases with $\bar{u}_{2m}$ and can be fairly represented by

$$\overline{w'T'} = 0.042\ \bar{u}_{2m} \quad . \tag{71}$$

The lines shown in Figures 4 through 6, 8, and 9 are drawn by visual observation.

The following sets of figures are based on data taken during the late autumn, winter, and early spring of 1992 (in all 11 sets of data). During these periods, the ground was either covered with snow or ice, or it was bare but either partially frozen or frozen. Figure 10 shows the relation

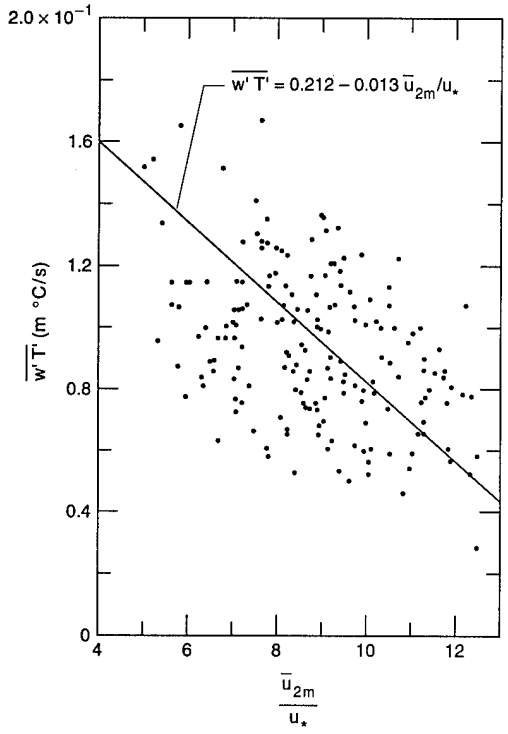

Figure 8. Variation of covariance $\overline{w'T'}$ *with* $\bar{u}_{2m}/u_*$.

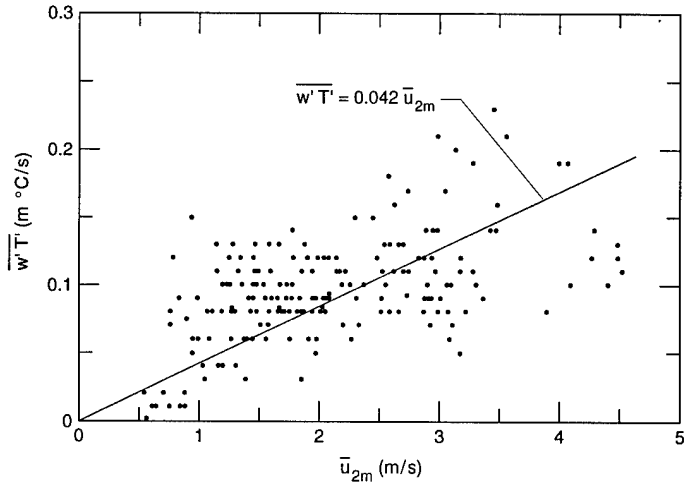

Figure 9. Variation of covariance $\overline{w'T'}$ *with* $\bar{u}_{2m}$.

between u_* and $\bar{u}_{2m}$, and a least-squares relation was developed as

$$u_* = 0.079\ \bar{u}_{2m}\ . \tag{72}$$

The dependence of u_* on $\bar{u}_{2m}$ is somewhat weaker when it is compared with that shown in Figure 4 (i.e., $u_* = 0.113\ \bar{u}_{2m}$). It can be said that over snow, ice, or partially frozen ground the value of u_* is significantly lower because there is less-intense turbulence over snow or ice than over a grass field (~2–3 cm tall).

Figures 11 shows the relation of $\sigma_{w'}$ and $\sigma_{u'}$ with $\bar{u}_{2m}$. The linear least-squares correlation can be expressed as

$$\sigma'_w = 0.113\ \bar{u}_{2m} \tag{73}$$

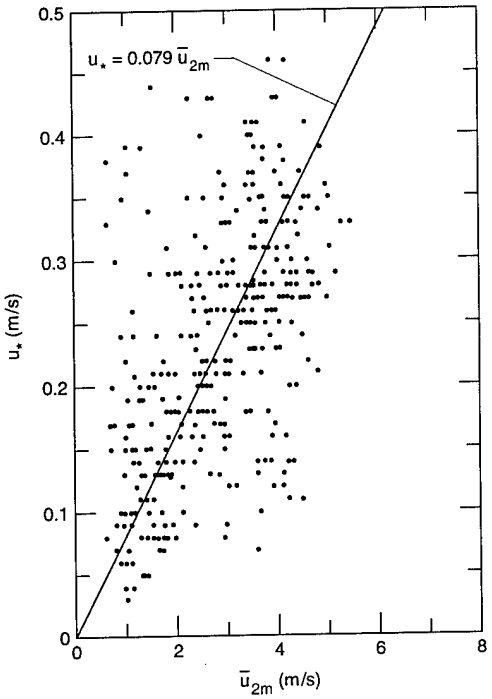

Figure 10. Variation of u_* with $\bar{u}_{2m}$ based on data taken in late fall, winter, and early spring.

and

$$\sigma'_u = 0.35\ \bar{u}_{2m}\ . \tag{74}$$

The value of 0.113 is slightly lower than that in eq 66, but the value of 0.35 is identical to the one given in eq 67. Figure 12 shows the variation of $\sigma_{u'}$ and u_* for the same measurement period and can be expressed by

$$\sigma_{u'} = 3.68\, u_*\ , \tag{75}$$

which is more or less the same as the relation shown in eq 68.

Figure 13 shows the variation of covariance $\overline{w'T'}$ with $\bar{u}_{2m}$. It can be represented by

$$\overline{w'T'} = 0.014\ \bar{u}_{2m}\ . \tag{76}$$

The constant 0.014 is only one third of the value given in eq 71. Neglecting the effect of variation of ρ and c_p with temperature and atmospheric pressure, the sensible heat flux is only one third of the value during the late spring to early summer.

Though the data points in all these figures are scattered to a great extent, the least-squares correlation coefficients of all these linear relations, i.e., eq 71–76 are greater than 0.8313 (as high as 0.9716 for $\sigma_{u'}$ vs. $\bar{u}_{2m}$). It indirectly indicates that $\bar{u}_{2m}$ is the predominant factor in correlating this type of data.

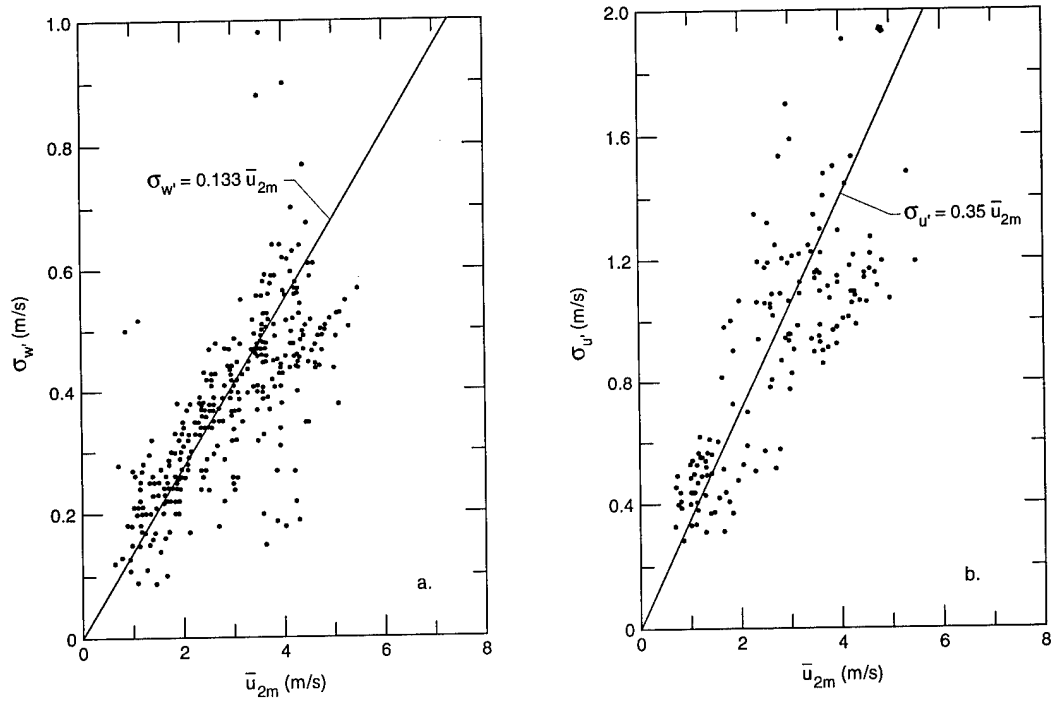

Figure 11. Standard deviations $\sigma_{w'}$ (a) and $\sigma_{u'}$ (b) as a function of $\bar{u}_{2m}$ based on data taken in late fall, winter, and early spring.

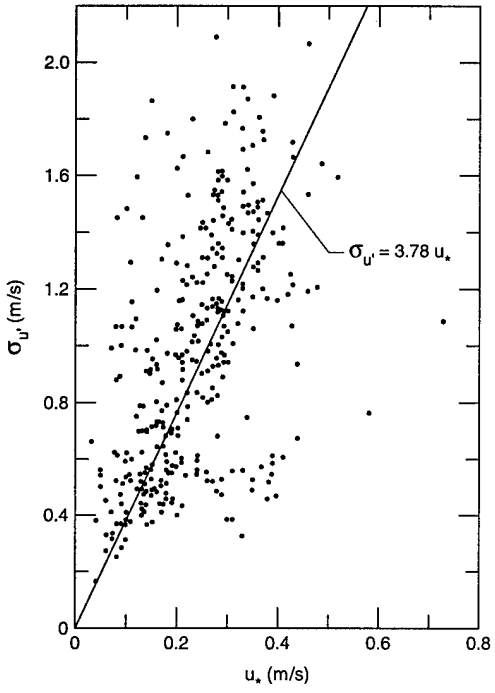

Figure 12. Standard deviation $\sigma_{u'}$ as a function of u_* based on data taken in late fall, winter, and early spring.

Tests under stable conditions were hard to realize. A stable surface air layer with very calm winds usually prevails soon after sunset. However, the magnitude of the sensible heat flux under stable conditions is very low, and the few data points collected during this period exhibited a much greater dispersion than in the case of unstable conditions. Figure 14 shows the relation of $-\overline{w'T'}$ with $\bar{u}_{2m}$ (we consider the heat flux from the air to the snow or ground surface to be negative). The least-squares analysis only gives a correlation coefficient of 0.0751, indicating practically no correlation between $-\overline{w'T'}$ and $\bar{u}_{2m}$.

The ratio of $\sigma_{w'}/u_*$ may be expressed in terms of a universal function of the stability parameter z/L according to the similarity theory. Figure 15 shows the variation of $\sigma_{w'}/u_*$ with z/L, clearly exhibiting the features of the ratio varying over a range of z/L from $-100 \le z/L \le 100$ (in most of the past studies, the range of z/L is from $-1 \le z/L \le 10$). As in other studies, there is a great dispersion of data (all the overlapping values of $\sigma_{w'}/u_*$ are omitted in the figure). No values of $\sigma_{w'}/u_*$ fall into the range of $-0.01 < z/L < 0.01$ due to lack of near-neutral conditions. For unstable conditions over the whole range of $-z/L$ covered in this study, the value of $\sigma_{w'}/u_*$ can be fairly represented by

$$\frac{\sigma_{w'}}{u_*} = 1.3\left[1-\left(\frac{z}{L}\right)\right]^{1/3}, \tag{77}$$

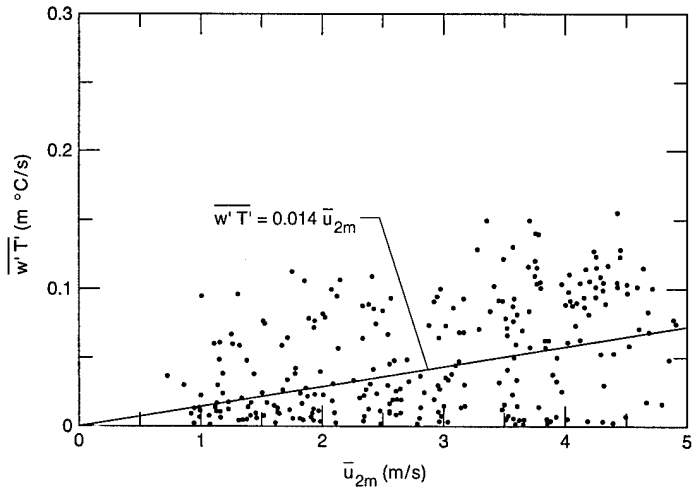

Figure 13. Covariance $\overline{w'T'}$ as a function of $\bar{u}_{2m}$ during late fall, winter, and early spring.

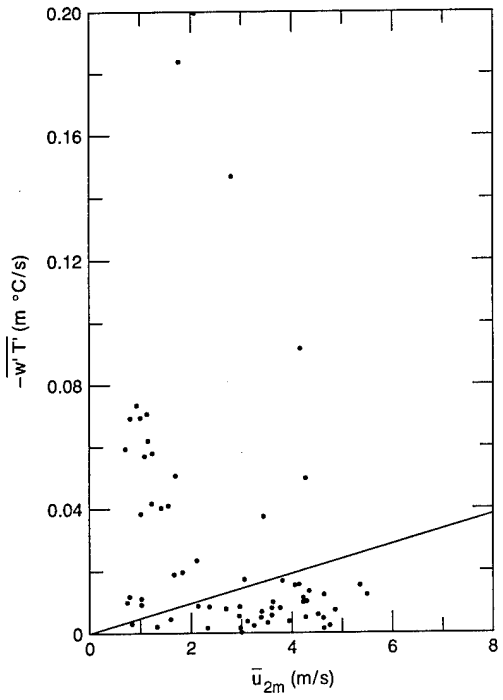

Figure 14. Covariance $-\overline{w'T'}$ as a function of $\bar{u}_{2m}$ during late fall, winter, and early spring.

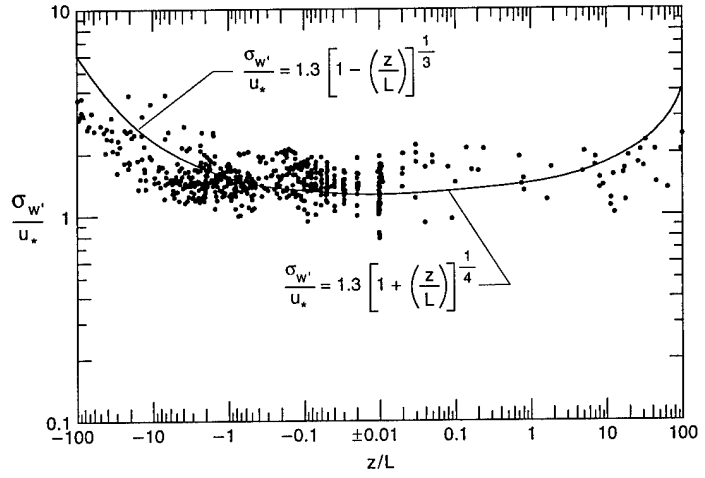

Figure 15. Variation of $\sigma_{w'}/u_*$ with stability parameter z/L.

Table 3. Comparison of the ratio $\frac{\sigma_{w'}}{u_*}$ under neutral conditions.

Test field	$\frac{\sigma_{w'}}{u_*}$	*Height of measurement (m)*	*References*
Over the sea	1.23	6.4, 12.5	Natio (1978)
Over the sea	1.32	8	Pond et al. (1971)
Over the sea	1.47	1.4—4.5	Miyake et al. (1970)
Over land	1.53	1.4	McBean (1970)
Over tall grass	1.32	1.6, 4.3, 12.3, 29.5	Kai (1982)
Over snow, frozen ground, and partially frozen ground	1.30	2	This study

which is different from the expression proposed by Panofsky et al. (1977) for $z/L \geq -1.0$, i.e.,

$$\frac{\sigma_{w'}}{u_*} = 1.3\left[1-\left(\frac{z}{L}\right)\right]^{1/3}, \tag{78}$$

but Kai (1982) claimed that his data can be represented rather well by the above expression.

For stable regions (i.e., $0.01 \leq z/L \leq 100$), even though there are less data available, a similar expression with an exponent of 1/4 instead of 1/3 can be derived as

$$\frac{\sigma_{w'}}{u_*} = 1.3\left[1+3\left(\frac{z}{L}\right)\right]^{1/4}. \tag{79}$$

Table 3 shows the comparison of the ratio $\sigma_{w'}/u_*$ with other results under neutral conditions. It can be seen that the ratio of $\sigma_{w'}/u_*$ taken from this study is within the range reported by all the investigators listed in Table 3. Even though the friction velocity u_* varies with the homogeneity of the upwind fetch and the surface roughness, the ratio of $\sigma_{w'}/u_*$ from this study (under neutral conditions) falls nevertheless within the limits reported by other investigators. This value, along with the relations given for u_* vs. $\bar{u}_{2m}$ (eq 65), $\sigma_{w'}$ vs. $\bar{u}_{2m}$ (eq 66), and $\sigma_{w'}$ vs. u_* (eq 69), certainly gives credence to the results obtained from this preliminary investigation. The agreement provides confidence in carrying out the essential purpose of this investigation, i.e., the use of the eddy correlation technique to determine the sensible heat flux.

Table 4 shows a summary of the computed sonic results. It can be seen that, with the exception of plots of $\sigma_{w'}$ vs. u_* and $-\overline{w'T'}$ vs. $\bar{u}_{2m}$, the slope of all other plots decreases slightly as the test runs extended from 30 May 1991 to 15 April 1992, with the lowest slope for the test runs conducted from 19 December 1991 to 15 April 1992. It seems that in the presence of snow or ice-covered or frozen ground, friction velocity u_*, standard deviations $\sigma_{w'}$, $\sigma_{u'}$, and the covariance $\overline{w'T'}$ are slightly less dependent on $\bar{u}_{2m}$. In other words, for the same value of $\bar{u}_{2m}$, the values of u_*, $\sigma_{w'}$, $\sigma_{u'}$, and $\overline{w'T'}$ are reduced somewhat as the tests progressed from spring to winter.

B. Sensible heat flux correlation

To facilitate the practical use of the sensible heat flux data presented in Table 4, a dimensionless analysis is needed to extend the results for other test conditions. For the test period from 19 December 1991 to 15 April 1992, the variation of $\overline{w'T'}$ (positive for unstable conditions or for heat rising from the surface) with $\bar{u}_{2m}$ was given in eq 76 as

$$\overline{w'T'} = 0.014\ \bar{u}_{2m}$$

Table 4. Summary of linear correlation of computed sonic results from 1991–1992.

Test period	*9105301331 to 9108201600*		*9105301331 to 9112111530*		*9105301331 to 9204151725*		*9105301331 to 9104151725*	
Type of plot	*Slope*	*Correlation coefficient*	*Slope*	*Correlation coefficient*	*Slope*	*Correlation coefficient*	*Slope*	*Correlation coefficient*
u_* vs. $\bar{u}_{2m}$	0.1034	0.9722	0.0994	0.9664	0.0893	0.9337	0.0785	0.8992
u_* vs. $\bar{u}_{2m}$	0.1614	0.9845	0.1572	0.9721	0.1456	0.9241	0.1330	0.8701
$\sigma_{u'}$ vs. $\bar{u}_{2m}$	0.3723	0.9816	0.3635	0.9812	0.3564	0.9765	0.3487	0.9716
$\sigma_{u'}$ vs. u_*	3.4431	0.9638	3.4710	0.9634	3.5940	0.9420	3.7788	0.9182
$\overline{w'T'}$ vs. $\bar{u}_{2m}$	0.0398	0.9052	0.0250	0.8649	0.0241	0.8160	0.0140	0.8313
$-\overline{w'T'}$ vs. $\bar{u}_{2m}$	0.00005	0.8049	0.0003	0.1583	0.0023	0.0746	0.0045	0.0751

in which the constant 0.014 contains a dimension of °C. Multiply both sides of eq 76 by ρ, c_p, and z and divide by ΔT, the difference in temperature between the measurement height and the surface (which was not measured in this study because there is no proven and reliable technique to measure the snow surface temperature). The following equation is obtained:

$$Nu = \frac{0.014}{\Delta T} RePr \ , \tag{80}$$

where Nu is the Nusselt number defined as $Hz/k\Delta T$, Re is the Reynolds number $\bar{u}\rho z/\mu$, and Pr is the Prandtl number, $c_p\mu/k$. The essential purposes in expressing the results in terms of the dimensionless Nusselt, Reynolds, and Prandtl numbers is to include the effect of air temperature on the variation of physical properties of air such as viscosity μ, density ρ, specific heat c_p, and thermal conductivity k. Although eq 80 is dimensionless, it is not in typical dimensionless form because it contains the term ΔT (which was introduced to define the Nusselt number and was not measured during the test). However, as shown in Table 4, the correlation coefficients are rather high, demonstrating that quantities such as u_*, $\sigma_{w'}$, $\sigma_{u'}$, and $\overline{w'T'}$ are strongly dependent on $\bar{u}_{2m}$ alone. Although the tests were conducted over nearly a one-year period, the values of ΔT appear to vary within a small range, and subsequently a more or less identical correlation will be produced if the data ΔT is available and is used to evaluate the Nusselt number, where H is the heat flux, $\bar{u}$ is the mean horizontal wind speed, and z is the measurement height.

Since the value of Pr for the temperature range from 240 to 300 K can be approximated by

$$Pr = 0.97 - 0.0009T, \tag{81}$$

where T is air temperature in Kelvin (K), substituting eq 81 into eq 80 we have

$$Nu = \frac{0.014}{\Delta T} Re(0.97 - 0.0009\,T) \ . \tag{82}$$

As long as the mean wind speed $\bar{u}$ is known, along with the temperature at height z, even without the data on ΔT, heat flux H can be calculated from eq 82 because ΔT is also used in defining the Nusselt number Nu (i.e., $Hz/k\Delta T$), so we do not need to know the value of ΔT to calculate H from eq 82.

For an average temperature of 273.1 K during the winter months, eq 82 can be further simplified as

$$Nu = \frac{0.010}{\Delta T} Re \ . \tag{83}$$

On the other hand (Table 4), for the period from May to August 1991, and by assuming an average air temperature of 293 K, an expression of

$$Nu = \frac{0.028}{\Delta T} Re \tag{84}$$

can be derived. The value of ΔT does not come into the process to calculate heat flux H in either eq 82 or 84, so for the same value of Re values of H are about three times greater during the summer season than during the winter. For the whole year (May 1991–April 1992) based on the data shown in Table 4, the value of Nu can be expressed by

$$Nu = \frac{0.024}{\Delta T} Re(0.97 - 0.0009\,T). \tag{85}$$

Therefore, as long as the mean horizontal wind speed and the air temperature at the height of the sonic measurement are determined, the value of Re can be calculated and subsequently the heat flux H can be determined.

VII. COMPARISON OF SENSIBLE HEAT FLUX

Based on boundary layer integral analysis in conjunction with a study of heat flux over Arctic leads, Andreas (1977) presented a dimensionless relation relating the Nusselt number Nu to the products of the Stanton number St, the Reynolds number Re, and the Prandtl number Pr, as

$$Nu = St \cdot Re \cdot Pr, \tag{86}$$

in which the dimensionless groups are chosen to be defined as

$$Nu = \frac{Hx}{k(T_w - T_{0.5})}, \quad St = \frac{H}{\rho c_p \bar{u}_{0.5}(T_w - T_{0.5})}, \quad \text{and} \quad Re = \frac{\bar{u}_{0.5} x}{\nu},$$

where T_w is the surface water temperature, and $\bar{u}_{0.5}$ and $T_{0.5}$ are the mean wind speed and air temperature measured at 0.5 m above the lead at fetch x, respectively. All the other properties, i.e., ν, ρ, c_p, and k, are evaluated at T_w. Andreas's results were finally expressed either by

$$Nu = 0.18\, Re^{0.71} \tag{87}$$

or in linear form as

$$Nu = 2.24 \times 10^{-3}\, Re + 1120\,, \tag{88}$$

which was compared with the theoretical expression presented by Kays (1966) for flow over a constant-temperature flat plate, i.e.,

$$St = 0.0295\, Re^{-0.2}\, Pr^{-0.4}, \tag{89}$$

which is not in good agreement with the expression resulting by equating eq 87 and 86, i.e.,

$$St\, Re\, Pr = 0.18\, Re^{0.71} \tag{90}$$

or

$$St = 0.18\, Re^{-0.29}\, Pr^{-1}. \tag{91}$$

For $Pr = 0.714$, eq 91 becomes

$$St = 0.2521\, Re^{-0.29}, \tag{92}$$

which is quite different from Kay's theoretical expression (eq 89). By substituting $Pr = 0.714$, eq 89 becomes

$$St = 0.0338\, Re^{-0.2}, \tag{93}$$

Assuming eq 92 and 93 have a same exponent to Re, eq 92 gives about seven times larger values than Kay's theoretical expression (eq 93). Andreas also compared his findings with the theoretical expression developed by Schlichting (1968) for flow over a heated plate by assuming a drag coefficient of 1.76×10^{-3} and $Pr = 1.0$, i.e.,

$$Nu = 1.76 \times 10^{-3}\, Re \tag{94}$$

For a value of $Re = 2.94 \times 10^5$, we have a flux value H of 36 W/m^2 from eq 83. For the same value of Re and a ΔT of 20°C, eq 88 gives an H value of ~400 W/m^2, which is approximately 10 times higher than the value obtained from this study. But for the same values of Re and ΔT, eq 94 predicts a value of ~125 W/m^2, which is about one third of the 400 W/m^2 given by eq 88 and about three times larger than the 36 W/m^2 given by eq 83. However, it should be noted that in Andreas's field test not only is the temperature difference $(T_w - T_{0.5})$ always about 20°C, but the measurement

heights are also different. On the other hand, in this study, the ΔTs are much smaller, i.e., on the order of 2°C (or even less), thus creating much less intense convective heat transfer.

As in this study, Tanner and Green (1989) reported an average sensible heat flux value of 49 W/m^2. His field test was conducted 14–17 August, and four sonic anemometers were used (one for each post, but each installed at a different level). For a comparable period from May to August (Table 4 or eq 84), and for the same *Re* value of 2.95×10^5, a heat flux of about 142 W/m^2 can be found, which is about three times higher than the value calculated from eq 83 for tests over snow and frozen and partially frozen soil covered with thin ice. This value, however, is in quite good agreement with the average heat loss over Arctic leads of about 250 W/m^2 reported by Andreas (1977). The data given by Tanner and Green were not sufficient to give a statistical analysis, however, Andreas's data were taken from a test with a much more homogeneous field than the one in this study.

In a study on atmospheric turbulent flux over snow, Hicks and Martin (1972) measured eddy fluxes of momentum, sensible heat, and water vapor over Lake Mendota, Wisconsin, and reported, under stable atmospheric conditions, an average sensible heat flux of 9 W/m^2 for a wind speed of ~2.7 m/s and ΔT from surface to air at 2 m of approximately 3°C. This average heat flux was computed from a total of four 1-hour measurements, and flux varies from 4.2 to 11.9 W/m^2. In this study, for the period with snow or thin ice-covered surface, the heat flux was found to be on the order of 25 W/m^2, about twice the maximum value reported by Hicks and Martin. Since, as indicated, the test site is quite inhomogeneous due to the limited fetch length and other obstacles, it was very difficult to measure the sensible heat flux properly under stable atmospheric conditions. Stable conditions usually prevail during a clear night with calm wind, but under these conditions frost forms on the sonic head, inhibiting its sensitivity of measurement. Therefore, there are hardly any reliable means to measure this low heat flux. Nevertheless, the sensible heat flux under stable conditions for the period from May 1991 to April 1992 (Table 4) has a value of ~13 W/m^2, nearly identical to the value reported by Hicks and Martin (1972). It should be noted that even for a period of nearly a year, there was not sufficient data to make a valid statistical analysis (note the near-zero value of the correlation coefficient).

For unstable atmospheric conditions and for a grass-covered field, the sensible heat flux is found to be approximtely 90 W/m^2 (based on eq 84) for a wind speed of 2 m/s. Based on five sets of field measurements for a range of $0.02 < |z/L| < 0.6$, Dyer (1967) reported an average sensible heat flux of $H = 212\ \Delta\theta^{3/2}$ where $\Delta\theta$ is the potential temperature difference between heights of 1 and 4 m. In this study, the value of $\Delta\theta$ is on the order of 3°C. Therefore, based on Dyer's expression, the sensible flux is about ~600 W/m^2, which is about seven times greater than 90 W/m^2.

In a study involving measurements of evaporation and heat transfer in the lower atmosphere by an automatic eddy-correlation technique, Dyer (1961) conducted a great number of measurements of 5-min duration covering a 26-day period from January to March over a level pasture with wind speeds varying from 1.96 to 7.28 m/s, with a mean wind speed of 4.2 m/s. Because of the short response time of the sensing equipment (~0.3 s), he indicated that, for conditions of moderate and high instability, significant deficiencies in eddy-flux measurements will occur only with wind speeds exceeding 10 m/s. He reported an average sensible heat flux of 155 W/m^2 (during his test the wind speeds were mostly in the vicinity of 4 m/s; in only seven of the 26 tests were the wind speeds less than 4 m/s). Using 4 m/s as the mean wind speed in eq 84 (a correlation from this study), a heat flux of 180 W/m^2 results, which is in remarkably good agreement with the value of 155 W/m^2 reported by Dyer. He further stated that with measurements at a height of 4 m, minor surface irregularities of up to several tens of centimeters are clearly of no consequence, and, if sufficient fetch is available, great irregularities could be readily accommodated by increasing the height and period of observation. For stable conditions, Dyer (1961) reported a heat flux value of ~14 W/m^2, which is nearly identical to the value reported by Hicks and Martin (1972).

In a study dealing with differences between air and snow surface temperatures during snow evaporation, Bernier and Edwards (1989) reported an average heat flux of 16 W/m^2 transported from the air stream to the snow surface under stable conditions (based on a total measurement of 14 data points from 1030 to 1930 hr), which is about 7 W/m^2 higher than the value reported by Hicks and Martin (1972) and approximately 9 W/m^2 less than the value obtained from this study. Bernier and Edwards concluded that the sensible heat flux from air to snow is the essential source of the energy escaping from the snowpack surface through the latent heat flux. They concluded that snow surface temperatures are generally lower than the air temperature and therefore, based on their theoretical analysis, if the air and snow temperatures are equal and air temperatures are below 273 K, the heat flux will be overestimated. It should be noted, however, that the snow surface is rather ill-defined because of its dynamic nature, so it is hard to measure its temperature.

Bates and Gerard (1989) discussed the various alternative means to predict snow surface temperature. With the assumption that a measurement by an infrared radiometer was the snow surface temperature, they compared the temperature measured by thermistor/ thermocouple, the air temperature at 2 m, and the dew point temperature against the infrared temperature and concluded that the radiometer would provide the most accurate estimate of the snow surface temperature, followed in order by thermistor/thermocouple, the air temperature, and the dew point temperature.

De La Casiniere (1974) conducted studies on heat exchange over a melting snow cover with reported means of diurnal and nocturnal balance of sensible heat flux of 0.2 MJ/m^2 and 0.23 MJ/m^2, respectively, which are equivalent to 4.6 and 5.3 W/m^2, respectively (without a description of the test conditions, it is hard to compare these reported values with others).

In a comprehensive study of snow surface energy exchange, Male and Granger (1981) discussed extensively the numerous factors affecting the turbulent energy exchange over a snow surface. They made the following observations: a) there have been many studies involving energy transfer, covering all areas of the world and various sites, i.e., open, forested, mountain snowpacks, isolated snowpacks, etc.; b) most of the studies dealt with melting snow, especially on glacier snowpacks, and virtually all were area point studies; c) very few direct measurements of turbulent energy fluxes are available (estimates based on aerodynamic formulas do not constitute direct measurement); d) although a number of absolute values (measured or calculated) are reported, the general trend is to present results regarding the relative contributions of the various forms of energy transfers; and e) only a few investigations attempted to note any diurnal or seasonal trends and to describe similarities between their findings or those of others. They concluded that the majority of investigators estimate the turbulent sensible heat flux from the use of aerodynamic formulas derived with the assumption of steady turbulent flow of a viscous fluid over an infinite, uniform, and hydrodynamically rough surface, implying that the transfer is only in the vertical direction and is time-independent (inferring the vertical flux is constant with height). However, the extent to which the turbulent fluxes vary with height has been the subject of several investigations. Dyer (1968) reported a 16.8% departure from the surface value for the turbulent sensible and latent heat fluxes at the 16-m level. Haugen et al. (1971) reported that turbulent heat flux and shear stress are constant only to within 20% up to a height of 23 m.

The variation of heat flux with height may be more pronounced over snow and melting snow because of their high albedo and the limiting upper-bound temperature of 0°C. De La Casiniere (1974), Granger (1977), and Halberstam and Schieldge (1981) conducted measurements over melting snow and showed that temperature anomalies are introduced by radiative heating of the air above the snow surface. Because the upper-bound temperature is 0°C, the air over snow will be heated above the snow temperature, resulting in a stable profile, but if the air mass is cool, a temperature maximum is observed in the air layer 20–50 cm above the surface. In this situation, not only is the heat flux not constant with height, but it undergoes a reversal in direction at the level of the raised maximum.

Priestley (1959), on the other hand, points out that for an air layer being heated by radiation the sum of the radiant and turbulent fluxes is essentially constant with height; therefore, to estimate energy transfer over snow, one must ensure not only that the measurements of temperature and humidity are made above the level of the raised maximum temperature, but that a simultaneous radiation measurement is also included. Priestley suggested that we must be content with the total surface energy transfer rather than that of the individual surface fluxes.

Large-scale parameters, such as topography, altitude, season, and air mass, were considered in Male and Granger's (1981) analysis of snow surface energy exchange. For brevity and comparason, they expressed their summarized results in percentages of the total energy input, indicating not only different values from year to year at the same site, but also making it impossible to state which particular energy flux will dominate overwhelmingly or be negligible in any particular environment. They also indicate that not only topography but other factors such as the air mass and large-scale circulation affect the process of energy transfer. Therefore, it is difficult or even dangerous to classify sites in general as being either open, forested, or alpine, since physically similar sites with different geographical placement will necessarily have different air mass histories. For snow-covered prairies and large open sites, theoretical approximation expressions derived after taking into account the influences of stability and the possibility of radiative heating of the air above the snow can be used directly to estimate the energy fluxes at the surface. In a review study of snowmelt in a prairie environment, Male and Granger (1979) developed a number of empirical methods of estimating energy fluxes and their accuracies and noted that the air mass exerts a controlling influence on the relative magnitude of the various energy fluxes.

In the case of forest cover, turbulent flux measurements have received little attention either because wind, temperature, and humidity measurements have been difficult to obtain or because these fluxes have been ignored in the assumption that reduced wind speed results in near-negligible energy fluxes. This may be true in the region of northern Quebec, for Hendrie and Price (1978) pointed out that radiation alone provides an efficient predictor of the snowmelt, but farther south turbulent exchange is found to be more significant (at least during the melting season) because snowmelt is usually initiated by the movement of a warm air mass into the region. To estimate the advective component of snowmelt M_{af} under a forest canopy compared to the corresponding part of the M_a of an open locality, Kuz'min (1961) developed

$$M_{af} = (0.44 - 0.43\, p^{2)} M_a \tag{95}$$

for coniferous and

$$M_{af} = (0.45 - 0.15\, p^{2)} M_a \tag{96}$$

for deciduous, where p is the crown density of the canopy. Doty and Johnson (1969) reported 30% and 53% reductions in evaporation rates within aspen and coniferous stands, respectively, as compared with an open site.

Application of standard aerodynamic formulas to predict turbulent fluxes over a forest canopy has been reported by Federer and Leonard (1971) to be inappropriate, based on the fact that in subcanopy flow the sources of mechanical turbulence and sensible heat flux are distributed vertically through the canopy. Brutsaert (1979) formulates bulk mass and heat transfer coefficients for canopy flow but, as pointed out by Federer and Leonard (1971), the transfer characteristics are likely to be quite different.

In the case of an alpine environment, Obled and Harder (1979) reviewed studies of snowmelt in a mountain environment and listed a number of factors affecting the turbulent transfer of heat and water vapor over snow. Wind and temperature regimes in the mountain environment are complex and make the analysis of the boundary layer on the basis of local slope winds difficult. Martin (1975) provides a formulation for the katabatic wind profile and applies it to the calculation of the

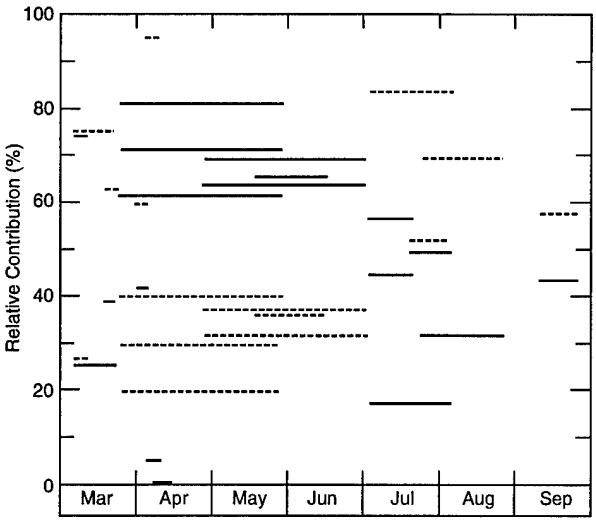

Figure 16. Relative contributions of the radiative (dashed line) and turbulent (solid line) energy transfer over snow as function of season (after Male and Granger 1981).

turbulent fluxes over snow. In general, however, due to the great variability of alpine winds with respect to type, space, and time, the type of analysis seems to be impractical for operational purposes, and hydrologists have usually resorted to the use of standard aerodynamic formulas in dealing with alpine snow fields and glaciers subjected to appropriate stability correlations.

Male and Granger (1981) graphically showed the relative contributions of radiative and turbulent energy transfers over a snow surface as functions of season and elevation. Figure 16 shows a large scatter in the relative contributions of the radiative and turbulent fluxes because melting of the low-level, shallow snowpacks, which melt quite early in the spring, depends largely on the energy content of the air mass present. On the other hand, deeper snowpacks that melt later in the year masked the effect of perturbations of the air masses and displayed the long-term trend of increased relative contribution of radiant energy. Figure 17 shows the effect of elevation on the relative contribution of energy fluxes. It can be seen that below 2000 m there is no correlation between elevation and the relative contribution of radiant and turbulent energy fluxes, indicating the influence of other factors such as topography or air mass. For elevations above 2000 m, there is an apparent decrease in turbulent flux contribution as the elevation increases. However, this trend seems to be valid only when the effect of other factors is negligible. In conclusion, it seems that there is not enough data to distinguish the influence of altitude and season on the relative contributions of radiant and turbulent energy transfers.

The influence of the air mass on the turbulent energy transfer was first reported by Sverdrup (1936) in his paper dealing with turbulent exchange with snow. He broadly classified his results in terms of the prevailing general weather conditions, i.e., a cold dry period is associated with a negative sensible heat transfer (heat leaving the surface) accompanied by evaporation from the snow surface; and warm, dry and wet periods are connected with a positive sensible heat transfer with evaporation from and condensation to the snow surface, respectively.

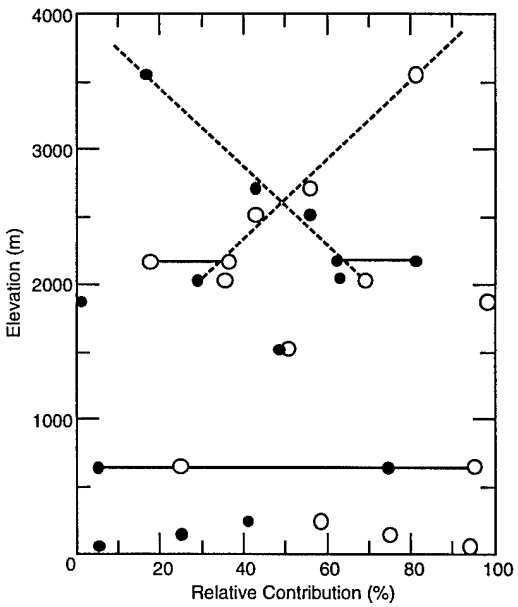

Figure 17. Influence of elevation on the relative contributions of radiative (open circles) and turbulent (solid circles) energy transfers over snow. Solid lines represent a range of values from a single location and dashed lines show the relationship between elevation (above 2000 m) and the relative contribution (after Male and Granger 1981).

The effect of energy and moisture contents of the air mass on evaporation/condensation has generally been overlooked, until Nyberg (1965) and Rylov (1969) made gravimetric measurements of evaporation/condensation at the snow surface and reported that the daily vapor flux is governed by the moisture content of the air mass. Hanaford and Howard (1975) dealt with an unusual snowmelt event due to an extreme warm upper air temperature. Granger (1977) and Granger and Male (1978) reported that the major melt-producing flux is due to radiation, and the advancement of the melt is governed by the energy content of the air mass. McKay and Thurtell (1978) confirmed the generalized results reported by Sverdrup (1936) and indicated the increase in the extent of evaporation during the transition from a warm to a cold air mass.

In general, it is fair to state that from the scatter and the variability of the results so far reported, based on a number of investigations under a variety of environmental and site conditions, the measurements of reliable and consistent sensible and latent heat exchanges have proven to be difficult even at well-instrumented sites. Furthermore, techniques or methods for extrapolating results from a small local measurement to larger areas, after taking into account the variations of elevation, latitude, state of the air mass, or topographical characteristics, have not been successfully developed.

Accurate information on sensible and latent heat and net radiative heat flux along with the heat transfer processes within the snow medium would be needed to calculate the snow surface temperature. This is largely due to the fact that the snow surface itself is so ill-defined that any intrusive measurement device, regardless of how small the sensing probe is, will disturb the surface structure, so it is uncertain whether the device is measuring the temperature of the snow grain or the air temperature of the void space enclosed by the snow grains. Male and Granger (1981) stated that investigations of large-scale or air mass influences on turbulent energy exchanges are likely to yield more practical results than investigations that are confined to a few meters above the snow surfaces. They also claim that research on air mass scale should give better insight into the factors governing changes in sensible and latent heat flux, because such studies are aimed at the cause rather than at an effect.

VIII. CONCLUSIONS

As indicated in section V, Experimental, the field site was chosen primarily for its convenience. The site is small, it is elevated on the west and north, and it definitely does not meet the fetch length requirement for eddy-correlation-type measurements. However, as indicated in section VI, Results and Discussion, the plots u_* vs. $\bar{u}_{2m}$ (Fig. 4) and $\sigma_{w'}$ vs. $\bar{u}_{2m}$ (Fig. 5a) are nearly identical to the results reported by Kai (1982), who used more sophisticated and modern sonic anemometers (three-dimensional) and a greater circular test field (160 m diameter). These surprisingly good agreements give much credence to our sensible heat flux results.

As indicated in section VII, Comparison of Sensible Heat Flux, a number of investigators have attempted to measure the sensible heat flux over a variety of terrains and environmental conditions but, due to the nature of the constantly changing atmosphere, there is really no way to apply the results obtained under a specific set of conditions to any specific combination of conditions. In other words, it is not possible to derive formulas to predict the sensible heat flux for areas other than the place or area where the measurement was made.

Though the sensible heat flux results obtained thus far from this study are rather preliminary and limited, the expressions derived as shown in eq 83 and 84 can be easily used to estimate the sensible heat flux as long as the mean wind speed and the mean air temperature at measurement height z are given. Since the snow surface temperature (in fact, any surface temperature) can hardly be determined without the introduction of errors, there is no easy way to evaluate the temperature difference between surface and the height of the measurement. However, by looking at the definition of

$Nu = Hz/k\Delta T$ and eq 83 and 84, it is clearly shown that we do not need to know the value of ΔT to calculate the value of sensible heat flux H.

Table 4 clearly shows the variations of $\overline{w'T'}$ with $\bar{u}_{2m}$ over a period of one year. The slope varies from 0.0298 for the measurements made from May to August to 0.014 for the period from December to the next April. In the May–August period, the sensible heat flux is about three times greater than the value calculated for the December–April period for a given Reynolds number Re. In other words, for a same mean wind speed $\bar{u}_{2m}$, the friction velocity u_* is lower over snow-covered ground than over grass-covered ground. This is evidenced in the variation of $\overline{w'T'}$ with the ratio of $\bar{u}_{2m}/u_*$ (Fig. 8). This trend can also be seen from Table 4 in which the slopes of the relation between u_* vs. $\bar{u}_{2m}$, $\sigma_{w'}$ vs. $\bar{u}_{2m}$, and $\sigma_{u'}$ vs. $\bar{u}_{2m}$ are slightly lowered as the test period expanded from May to August, December and then to April. The slopes of the relation between $\sigma_{u'}$ vs. u_* (Table 4) increases slightly as the test period progressed as was expected, i.e., to have the same value of u_* during the winter period (in this case December to April). It needs a higher value of mean wind speed $\bar{u}_{2m}$ and thereby creates a higher value of standard deviation of fluctuating velocity in the horizontal direction.

Though the study reported here is preliminary in nature, it has clearly established the fact that the sensible heat flux determined during the winter months or during snow- or ice-covered ground is about only one third of the value obtained during spring and summer months, i.e., over grass-covered ground. Therefore it is speculated that the use of expressions involving temperature and mean velocity gradients evaluated at measurement height z to estimate sensible heat flux from equations such as eqs 21 or 31 will definitely introduce a significant error because these equations are derived without the consideration of snow surface as a lower-surface boundary.

For sensible heat flux determined under stable conditions (which exists mostly at night under calm wind conditions), the data are much more scarce and showed a much greater dispersion, discussed in section VII, Comparison of Sensible Heat Fluxes. For the case of stable atmospheric conditions, Hicks and Martin (1972) reported an average value of 9 W/m^2 (for a mean wind speed of 2.7 m/s and ΔT of 3°C), which is about one third of the value obtained from this study under approximately the same test conditions (i.e., 27 W/m^2) (but for a period of one year, the heat flux reduces to 13 W/m^2, which is close to the value of 14 W/m^2 reported by Dyer (1961) as well as of 16 W/m^2 reported by Bernier and Edwards (1989).

For unstable atmospheric conditions, Dyer (1961) conducted sensible heat flux measurements over level pasture land with a mean wind speed of 4.2 m/s and reported a heat flux value of 155 W/m^2, which is nearly identical to the value of 180 W/m^2 calculated from eq 84 based on the present study. This close agreement may be accidental, because in another study Dyer (1967) derived an expression representing the sensible heat flux by $H = 212\,\Delta\theta^{3/2}$ (W/m^2). With $\Delta\theta$ on the order of 3°C, the value of H will be on the order of ~1100 W/m^2, which is about seven times greater than the value reported by Dyer (1961) as well as the value calculated based on eq 84.

In summary, based on several past studies as well as the present one, it can be concluded that not only does sensible heat flux depend on a number of factors, but it is difficult to obtain consistent results because of the constant changing of the atmosphere. The fact is that even during an averaging period of 10 minutes the wind speed and its direction vary greatly. Therefore, the fundamental assumption of constant, steady, and homogeneous upwind flow never can be realized in the field measurement to satisfy the condition of a so-called constant flux surface layer. It is expected that the results obtained with the eddy-correlation technique will provide a much more reasonable estimation for the sensible heat flux than the other methods discussed in section III, Computation of Turbulent Fluxes. Due to the constantly changing atmospheric dynamics, the steady, homogeneous surface layer flow will never be realized in field measurements to ensure the existence of the constant flux layer. Localized or regional measurements, which are used in this study, may still provide a much more reliable method to find the sensible heat flux needed for surface energy balance calculations.

LITERATURE CITED

Andreas, E.L. (1977) Observations of velocity and temperature and estimates of momentum and heat fluxes in the internal boundary layer over arctic leads. Ph.D. dissertation, Oregon State University.

Andreas, E.L, C.A. Paulson, R.M. Williams, R.W. Lindsay and J.A. Businger (1979) The turbulent heat flux from arctic leads. *Boundary Layer Meteorology*, **17**: 57–91.

Anderson, E.C. (1976) A point energy and mass balance model of a snow cover. NOAA Technical Report NWS 19, U.S. Department of Commerce.

Bates, R.E. and S. Gerard (1989) Snow-surface temperature analysis. In *Proceedings of the 46th Annual Eastern Snow Conference, Quebec City, Quebec, 8–9 June*, p. 109–116.

Bernier, P.Y. and G.C. Edwards (1989) Difference between air and snow surface temperature during snow evaporation. In *Proceedings of the 46th Annual Eastern Snow Conference, Quebec City, Quebec, 8–9 June*, p. 117–120.

Biltoft, C.A. and J.E. Gaynor (1987) Comparison of two types of sonic anenometers and fast response thermometers. In *6th Symposium on Meteorological Observations and Instrumentation, AMS, Boston, Massachusetts*, p. 173–176.

Brutsaert, W. (1972) Radiation, evaporation and the maintenance of turbulence under stable conditions in the lower atmosphere. *Boundary Layer Meteorology*, **2**: 309–325.

Brutsaert, W. (1979) Heat and mass transfer to and from surface with dense vegetation or similar permeable roughness. *Boundary Layer Meteorology*, **16**: 365–388.

Businger, J.A. (1973) Turbulent transfer in the atmospheric surface layer. In *Workshop on Micrometeorology* (D.A. Haugen, Ed.), American Meteorological Society, p. 67–100.

Businger, J.A., J.C. Wyngaard, Y. Izumi and E.F. Bradley (1971) Flux-profile relationships in the atmospheric surface layer. *Journal of the Atmospheric Sciences*, **28**: 181–189.

De La Casiniere (1974) Heat exchange over a melting snow surface. *Journal of Glaciology*, **13**(67): 5–72.

Deardorff, J.W. (1968) Dependence of air–sea transfer coefficients on bulk stability. *Journal of Geophysical Research*, **73**(8): 2549–2557.

Doty, R.D. and R.S. Johnson (1969) Comparison of gravimetric measurements and mass transfer computations of snow evaporation beneath selected vegetation canopies. *37th Annual Meeting of the Western Snow Conference, Salt Lake City, Utah.*

Dyer, A.J. (1961) Measurement of evaporation and heat transfer in the lower atmosphere by an automatic eddy-correlation technique. *Quarterly Journal of the Royal Meteorological Society*, **87**: 401–412.

Dyer, A.J. (1967) The turbulent transport of heat and water vapor in an unstable atmosphere. *Quarterly Journal of the Royal Meteorological Society*, **93**: 501–508.

Dyer, A.J. (1968) An evaluation of eddy flux variation in the atmospheric boundary layer. *Journal of Applied Meteorology*, **1**: 845–850.

Dyer, A.J. and B.B. Hicks (1970) Flux gradient relationships in the constant flux layer. *Quarterly Journal of the Royal Meteorological Society*, **96**: 715–721.

Federer, C.A. and R.E. Leonard (1971) Snowmelt in hardwood forests. Paper presented at the 28th Annual Meeting of the Eastern Snow Conference, Fredrickson, New Brunswick.

Granger, R.J. (1977) Energy exchange during melt of a prairie snowcover. M.S. thesis, Department of Mechanical Engineering, University of Saskatchewan, Saskatoon, Canada.

Granger, R.J. and D.H. Male (1978) Melting of a prairie snowcover. *Journal of Applied Meteorology*, **17**(12): 1833–1842.

Halberstam, I. and J.P. Schieldge (1981) Anomalous behavior of the atmospheric surface layer over a melting snowpack. *Journal of Applied Meteorology*, **20**: 255–265.

Hanaford, J.F. and C.H. Howard (1975) Upper air data as a parameter in estimating snowmelt runoff. *43rd Annual Meeting of the Western Snow Conference, Coronado, California.*

Haugen, D.A., J.C. Kaimal and E.F. Bradley (1971) An experimental study of Reynolds stress and heat flux in the atmospheric surface layer. *Quarterly Journal of the Royal Meteorological Society*, **97**: 68–180.

Hendrie, L.K. and A.G. Price (1978) Energy balance, snowmelt and runoff in a leafless deciduous forest. In *Proceedings of the Perch Lake Study Symposium/Workshop*, p. 3–26, AECL–6404, At. Engineering of Canada, Ltd., Chalk River, Ontario.

Hicks, B.B. (1970) The measurement of atmospheric fluxes near the surface. *Journal of Applied Meteorology*, **9**: 386–388.

Hicks, B.B. and H.C. Martin (1972) Atmospheric turbulent fluxes over snow. *Boundary Layer Meteorology*, **2**: 496–502.

Kai, Kenji (1982) Statistical characteristics of turbulence and the budget of turbulent energy in the surface boundary layer, No. 1. Environmental Research Center, University of Tsukuba, Ibaraki, Japan.

Kaimal, J.C., J.C. Wyngaard, Y. Izumi and O.R. Cote (1972) Spectral characteristics of surface layer turbulence. *Quarterly Journal of the Royal Meteorological Society*, **98**: 563–589.

Kays, W.M. (1966) *Convective Heat and Mass Transfer.* New York: McGraw–Hill.

Kristensen, L. and D.R. Fitzjarrald (1984) The effect of line averaging on scalar flux measurement. *Journal of Atmospheric Oceanic Technology*, **1**(2): 138–146.

Kuz'min, P.P. (1961) Protsess tayaniya shezhnogo pokrova, Gidrometeorologicheskoe Izdatel'stvo, Leningrad (English translation: "Melting of snow cover," Israel Program for Scientific Translations (TT71–50095), 290 P. Jerusalem)

Lumley, J.L. and H.A. Panofsky (1964) *The Structure of Atmospheric Turbulence.* New York: Interscience.

Lunardini, V.J. (1981) *Heat Transfer in Cold Regions.* New York: Van Nostrand Reinhold Co.

Male, D.H. and R.J. Granger (1979) Energy and mass transfer at the snow surface in a prairie environment. In *Proceedings of a Meeting on Modeling of Snow Cover Runoff, 26–28 September 1978, Hanover, New Hampshire* (S.C. Colbeck and M. Ray, Ed.). USA Cold Regions Research and Engineering Laboratory, Special Report 79-36, p. 101-124.

Male, D.H. and R.J. Granger (1981) Snow surface energy exchange. *Water Resources Research*, **17**(3): 609–627.

Martin, S. (1975) Wind regimes and heat exchange on Glacier de Saint-Sorlin. *Journal of Glaciology*, **14**(70): 91–105.

McBean, G.A. (1970) The turbulent transfer mechanisms in the atmospheric boundary layer. Ph.D. thesis, University of British Columbia.

McKay, D.C. and G.W. Thurtell (1975) Measurement of the energy fluxes involved in the energy budget of a snow cover. *Journal of Applied Meteorology*, **17**: 339–349.

McVehil, G.E. (1964) Wind and temperature profiles near the ground in stable conditions. *Quarterly Journal of the Royal Meteorological Society*, **90**: 136–146.

Miyake, M., M. Donelan, G.A. McBean, C. Paulsen, F. Badgley and E. Leavitt (1970) Comparison of turbulent fluxes over water determined by profile and eddy correlation techniques. *Quarterly Journal of the Royal Meteorological Society*, **96**: 132–137.

Monin, A.S. and A.M. Obukhov (1954) Basic laws of turbulent mixing in the surface layer of atmosphere. *Akad. Nauk. SSSR, Trudy Geofizicheskii Institut*, **24**(151): 163–187.

Natio, G. (1978) Direct measurements of momentum and sensible heat fluxes at the tower in the open sea. *Journal of the Meteorological Society, Japan*, **56**: 25–34.

Nyberg, A. (1965) A study of evaporation and the condensation at a snow surface. *Ark. Geofys.*, **4**(30): 577–590.

Obled, C. and H. Harder (1979) A review of snow melting in the mountain environment. In *Proceedings of a Meeting on Modeling of Snow Cover Runoff, 26–28 September 1978, Hanover, New Hampshire* (S.C. Colbeck and M. Ray, Ed.). USA Cold Regions Research and Engineering Laboratory, Special Report 79-36, p. 179–204.

Oke, T.R. (1970) Turbulent transport near the ground in stable conditions. *Journal of Applied Meteorology*, **9**: 778–786.

Panofsky, H.A., H. Tennekes and J.C. Wyngaard (1977) The characteristics of turbulent velocity components in the surface layer under convective conditions. *Boundary Layer Meteorology,* **11**: 335–361.

Pond, S., G.T. Phelps, J.E. Paquin, G. McBean and R.W. Stewart (1971) Measurements of the turbulent fluxes of momentum, moisture and sensible heat over the ocean. *Journal of the Atmospheric Sciences*, **28**: 910–917.

Priestley, C.H.B. (1959) *Turbulent Transfer in Lower Atmosphere*. Chicago: University of Chicago Press.

Pruitt, W.O., D.L. Morgan and F.J. Lawrence (1971) Evaluation of eddy-transfer coefficients and diabatic-profiles function under turbulent flow in lower atmosphere, Chapter III. Final Technical Report, ECOM-68-G10-F, University of California, Davis, California (AD 721–301), p. 15–35.

Richardson, L.F. (1920) The supply of energy from and to atmospheric eddies. *Proceedings of the Royal Society of London*, Series A, **97**: 354–373.

Rylov, S.P. (1969) Snowcover evaporation in the semi-desert zone of Kazakhstan. *Sov. Hydrol. Sel. Rap.,* **3**: 258–270.

Schlichting, H. (1968) *Boundary Layer Theory*. 6th edition (Translation, J. Kestin). New York: McGraw–Hill.

Sverdrup, H.V. (1936) The eddy conductivity of the air over a smooth snow field—Results of the Norwegian–Swedish Spitzbergen Expedition in 1934. *Geofys. Publ.*, **11**(7): 1–69.

Swinbank, W.C. (1951) The measurement of vertical transfer of heat and water vapor by eddies in the lower atmosphere. *Journal of Meteorology*, **8**(3): 135–145.

Swinbank, W.C. (1964) The exponential wind profile. *Quarterly Journal of the Royal Meteorological Society*, **90**(384): 119–135.

Swinbank, W.C. (1968) A comparison between predictions of dimensional analysis for the constant flux layer and observations in unstable conditions. *Quarterly Journal of the Royal Meteorological Society*, **94**: 460–467.

Swinbank, W.C. and A.J. Dyer (1967) An experimental study in micrometeorology. *Quarterly Journal of the Royal Meteorological Society*, **93**: 494–500.

Tanner, B.D. and J.P. Green (1989) Measurement of sensible heat and water vapor fluxes using eddy-correlation methods. Final report prepared for U.S. Army Dugway Proving Ground. Logan, Utah: Campbell Scientific Inc.

Tanner, B.D., M.S. Tanner, W.S. Dugas, E.C. Campbell and B.L. Bland (1985) Evaluation of an operational eddy correlation system for evapotranspiration measurements. *National Conference on Advances in Evapotranspiration*, p. 87–99. American Society of Agricultural Engineering, St. Joseph, Michigan.

Thorpe, M.R., E.G. Bank and S.D. Smith (1973) Eddy correlation measurements of evaporation and sensible heat flux over arctic sea ice. *Journal of Geophysical Research*, **78**(18): 3573–3584.

Verma, S.B., N.J. Rosenberg and B.L. Blad (1978) Turbulent exchange coefficients for sensible heat and water vapor under advective conditions. *Journal of Applied Meteorology*, **17**: 30–338.

Warhaft, Z. (1976) Heat and moisture flux in the stratified boundary layer. *Quarterly Journal of the Royal Meteorological Society*, **102**: 703–704.

Webb, E.K. (1970) Profile relationships: The long linear range and extension to strong stability. *Quarterly Journal of the Royal Meteorological Society*, **96**: 67–90.

Wesley, M.L., G.W. Thurtell and C.B. Tanner (1970) Eddy correlation measurements of sensible heat flux near the earth's surface. *Journal of Applied Meteorology*, **9**: 5–50.

Wyngaard, J.C. (1973) On surface layer turbulence. In *Workshop on Micrometeorology* (D.A. Haugen, Ed.), American Meteorological Society, p. 101–149.

Yen, Y.-C. (1993) On the temperature distribution near a cold surface. USA Cold Regions Research and Engineering Laboratory, CRREL Report 93-19.

REPORT DOCUMENTATION PAGE

Form Approved
OMB No. 0704-0188

1. AGENCY USE ONLY (Leave blank)	2. REPORT DATE	3. REPORT TYPE AND DATES COVERED
	October 1995	

4. TITLE AND SUBTITLE

Sensible Heat Flux Measurements Near a Cold Surface

5. FUNDING NUMBERS

PE: 6.11.02A
PR: 4A161192AT24
TA: SS
WU: E09

6. AUTHORS

Yin-Chao Yen

7. PERFORMING ORGANIZATION NAME(S) AND ADDRESS(ES)

U.S. Army Cold Regions Research and Engineering Laboratory
72 Lyme Road
Hanover, New Hampshire 03755-1290

8. PERFORMING ORGANIZATION REPORT NUMBER

CRREL Report 95-22

9. SPONSORING/MONITORING AGENCY NAME(S) AND ADDRESS(ES)

Office of the Chief of Engineers
Washington, D.C. 20314-1000

10. SPONSORING/MONITORING AGENCY REPORT NUMBER

11. SUPPLEMENTARY NOTES

12a. DISTRIBUTION/AVAILABILITY STATEMENT

Approved for public release; distribution is unlimited.

Available from NTIS, Springfield, Virginia 22161

12b. DISTRIBUTION CODE

13. ABSTRACT (*Maximum 200 words*)

A unidirectional sonic anemometer with a fine-wire thermocouple in conjunction with a hot film anemometer were employed to measure the turbulent fluctuating velocities of w', u', and the fluctuating temperature T'. Covariances were evaluated to compute the turbulent heat flux and the friction velocity. Based on preliminary data, it can be noted that the values of fluctuating vertical velocity and temperature, the friction velocity, and the standard deviations of vertical and horizontal turbulent fluctuating velocities can all be correlated rather well with a single variable, i.e., the mean wind speed measured at a height of 2 m. In all the plots of friction velocity, vertical and horizontal turbulent fluctuating velocities, and the fluctuating vertical velocity and temperature vs. the mean wind speed at 2 m, the slopes are slightly lowered as the test season progressed from early summer to the winter. The most striking reduction can be observed in the case of the fluctuating vertical velocity and temperature vs. mean wind speed at 2 m. During the winter period, the slope is only about one third of that during the spring–summer period. In other words, under unstable conditions, for the same mean wind speed, the heat flux during the winter is only about one third of the flux that would have occurred during the spring–summer. Under stable conditions, the magnitude of the fluctuating vertical velocity and temperature is much smaller, and its value shows much greater dispersion. The values of fluctuating vertical velocity and temperature cannot be correlated in any meaningful manner, as is the case under unstable conditions, by the mean wind speed alone. Comparisons were made with the few existing measured data or with predictions from theoretical expressions, and they were found to be in fairly good agreement in some cases and to have large divergence in others.

14. SUBJECT TERMS

Energy balance
Fluctuating temperature
Fluctuating velocity
Sensible heat flux
Turbulence

15. NUMBER OF PAGES
52

16. PRICE CODE

17. SECURITY CLASSIFICATION OF REPORT	18. SECURITY CLASSIFICATION OF THIS PAGE	19. SECURITY CLASSIFICATION OF ABSTRACT	20. LIMITATION OF ABSTRACT
UNCLASSIFIED	UNCLASSIFIED	UNCLASSIFIED	UL